TECHNICAL REPORT NO. 594

Final Report

for

Development of an Electron Density Probe

(28 May 1965 - 28 February 1966)

Contract No. NAS5-9881

Prepared by

General Applied Science Laboratories, Inc.
Merrick and Stewart Avenues
Westbury, L. I., New York

for

National Aeronautics and Space Administration
Goddard Space Flight Center
Greenbelt, Maryland

June 1966

Project 8029

Total No. of Pages - ix & 125

Copy (119) of

TECHNICAL REPORT NO. 594

Final Report

for

Development of an Electron Density Probe

(28 May 1965 - 28 February 1966)

Contract No. NAS5-9881

By Hector Medecki
David Attwood

Prepared by

General Applied Science Laboratories, Inc.
Merrick and Stewart Avenues
Westbury, L. I., New York

for

National Aeronautics and Space Administration
Goddard Space Flight Center
Greenbelt, Maryland

Approved by: Robert W. Byrne
Robert W. Byrne
Vice President

June 26, 1966

SUMMARY

An electron density probe has been developed to measure from 10^{10} to 10^{14} e/cm^3. The probe is basically an open non-radiating electromagnetic cavity whose resonant frequency is uniquely related to the electron density of the surrounding medium. The calibration of this instrument has been performed with real and simulated plasmas.

Particular emphasis has been placed on an application in the separated flow region of a reentry Apollo spacecraft for a typical trajectory. The effects of heat transfer and diffusion of charged particles upon the operation of the probe have been estimated for those conditions. A preliminary design of a system for this in-flight measurement is presented.

ACKNOWLEDGMENTS

This work is based on an idea conceived by Dr. Manlio Abele, who directed the probe development through all phases. Mr. Robert Byrne is acknowledged for his skillful handling of the aerodynamic analysis as well as the inflight application.

The authors also wish to express their appreciation to Mr. Sulmo Mariano for computing the electromagnetic characteristics of the probe as well as the effects of charge diffusion. Dr. Masud Naraghi's design and construction of electrical gas discharge system is also appreciated. Thanks are due to Mr. Charles Sabin for his skillful construction of the probes. Finally, the authors acknowledge the collaboration of their fellow workers who are too numerous to mention individually.

TABLE OF CONTENTS

LIST OF FIGURES

NOMENCLATURE

c	speed of light in vacuum
e	electron charge
E	electric field intensity
f	cyclic frequency
h	enthalpy
H	magnetic field intensity
I	modified Bessel function of the first kind
J	Bessel function of the first kind
k	propagation constant
K	modified Bessel function of the second kind
n	electron density
N	Bessel function of the second kind
P	pressure
Q	quality factor
T	temperature
α	diffusion coefficient
δ	penetration depth
Δ	change of parameter value
ϵ	dielectric constant
$\varkappa$	refractive index
μ	permeability

ν	collision frequency
ω	angular frequency
λ	wavelength

Subscripts

c	critical condition, $\omega = \omega_p$
d	dielectric material
e	electrons
o	free space
p	plasma
r, θ, z	cylindrical coordinates
x, y, z	rectangular coordinates

Final Report

for

Electron Density Probe

I. Introduction

This report describes the work performed between May 28, 1965 and February 28, 1966 in the development of an electron density probe capable of operating in a superorbital shock tube tunnel, and while therein, be capable of measuring the electron density distribution within the separated flow region of a model of the Apollo spacecraft under superorbital reentry conditions at altitudes between 350,000 ft and 150,000 ft traveling at velocities from 36,000 to 10,000 fps (Ref. 1). The probe is designed to measure electron densities through the range 10^{10} to 10^{14} electrons per cubic centimeter (e/cm^3).

The principle of operation is based on the interaction between the plasma and the microwave electromagnetic field of an open nonradiating structure. The structure basically consists of a section of dielectric waveguide (Ref. 2) limited by two metallic reflecting surfaces. The propagation of an electromagnetic wave along a dielectric waveguide is known to depend on the complex dielectric constant of the surrounding medium (Ref. 3). Specifically, underdense plasmas introduce a perturbation of the evanescent field attached to the dielectric rod while overdense plasmas confine the electromagnetic field inside the dielectric except for a certain penetration of the field into the plasma itself. The resonant properties of these structures, namely the resonant frequency and Q, are related to the properties of the ionized gas. Consequently, electron densities and collision frequencies can be determined by referring to the equation for the dielectric constant of the plasma.

The range of operation of the probe depends on several factors including the desired spatial resolution, the obtainable quality factor and plasma boundary conditions. The interrelationship of these factors is discussed in succeeding chapters.

A cylindrical geometry has been chosen for this particular probe as there are no significant aerodynamic requirements to be satisfied and because this geometry lends itself to the desired polarization of the electromagnetic field in the region of interaction with the surrounding plasma.

II. Reentry Plasma Conditions

As the probe developed in this investigation is to be used in the separated flow region of a model of a reentering Apollo vehicle, it was necessary to anticipate the conditions which may exist there. With this in mind an attempt has been made to estimate the plasma properties of the gas in this region.

The basic reentry local flow conditions have been determined using the data given in NASA TM-X-705 in the same manner as was done in GASL TR-527 (Ref. 4). The stagnation point conditions were computed using real gas thermochemical equilibrium properties. The flow was assumed to expand from the stagnation conditions in equilibrium isentropic expansion to a point in the flow field where the Mach number is 2.5. It was assumed that the flow separates at this point and that the pressure in the separated region remained constant at this value. The enthalpy in the separated region was assumed to be related to the stagnation enthalpy by

$$h_{sep} = C \; h_{stag}$$

where

$$0.1 \leq C \leq 0.5$$

A Mollier diagram for equilibrium air was then used to determine the temperature in the separated region. In order to compute the ion-neutral collision frequency, use has been made of

$$\nu_i = 3.45 \times 10^{10}\ P\ T^{-1/2}$$

where P is the pressure in atmospheres and T is the temperature in degrees Kelvin. The electron-neutral collision frequency has been taken as

$$\nu_e = 165\ \nu_i$$

The results of this computation are shown in Fig. 1. It is seen here that the maximum electron density is approximately 10^{13} e/cm^3, and that the maximum collision frequency is approximately 7×10^8/sec. For a probe operating with a frequency of 10 KMHz (3 cm) this would give $n/n_c \sim 10$ and $\nu/\omega \sim 10^{-2}$.

III. The Slow Phase Velocity Structure

In conventional microwave transmission systems the electromagnetic energy is confined within a region of space bounded by conducting walls. Under certain conditions other types of waveguides may be used in which the energy is not rigidly confined, but rather is bound to a surface or structure. Such a guiding structure can support evanescent waves which are forms of electromagnetic energy propagating along the interface between two media with different physical properties. The electromagnetic field extends to infinity in the direction normal to propagation, but the energy density decreases in an exponential-like form so that in practice most of the energy of the wave is constrained to flow in the immediate neighborhood of the structure (Ref.5). Such a structure is characterized by a slow phase velocity, that is the phase velocity of propagation of the evanescent wave along the interface is slower than the phase velocity of a plane wave in the surrounding media (Refs.6 and 7).

The most common types of slow phase velocity structures are metallic helixes (Ref.8), metallic corrugated surfaces (Ref.9), and dielectric waveguides (Refs.10, 11 and 12). Each of these structures can support several electromagnetic modes. If a cylindrical geometry is adopted for the probe the losses due to current flowing between plasma and structure can be avoided by using a mode with no radial component of electric field. A mode of this type is the TE_{01n} which is easily excited in a circular dielectric waveguide. This was the deciding factor in choosing this element rather than a helix or corrugated structure.

In this mode the magnetic field has components in the axial and radial directions only, while the electric field has only an azimuthal component, which, as mentioned above, is symmetric. Within the rod itself the magnitude of the electric field has the form of a Bessel function of the first kind of order one, while in the region of the plasma it has the form of a Hankel function of the first kind and the first order. In other words the magnitude of this azimuthal electric field is zero at the center of the cylinder, builds up to a maximum within the rod and begins to decrease as one moves closer to the outer surface of the probe. Outside the rod, that is within the plasma, the electric field goes from the finite value at the wall within the dielectric to zero in an asymptotic form.

The variables to be manipulated in the design of a probe of this type are the free space wavelength λ_o, the effective wavelength along the axis of the dielectric rod λ_g, the radius of the dielectric rod r_o, its relative dielectric constant in the appropriate range of frequencies, ϵ_d, and the electromagnetic properties of the plasma. The relative dielectric constant of the plasma is related to the plasma properties by the equation

$$\epsilon_p = 1 - (n/n_c)(1 - i\,\nu/\omega)^{-1}$$

where n is the electron number density, n_c is the critical number density corresponding to a plasma frequency equal to the microwave frequency, ω is the angular microwave frequency, and ν is the electron collision frequency.

A qualitative description of the interrelationship between the parameters affecting the design of the probe follows. First of all the axial length of the probe must be equal to a whole number of half waveguide wavelengths (λ_g), that is the length ℓ should be taken as $\ell = (n/2)\lambda_g$ where n is any integer. From the point of view of spatial resolution it would be best to take n=1 for this would give a length on the order of a half inch, however this would maximize the end plate and coupling losses and diminish the Q of the probe. The end plates are the metallic surfaces at each end of the probe which form the boundaries of the resonant structure. As will be seen later the Q determines the minimum measurable electron density and hence must be kept as large as possible.

Another important factor is the ratio λ_g/λ_o which is related to the penetration of the electromagnetic wave inside the plasma. The condition $\frac{\lambda_g}{\lambda_o} \geq 1$ has to be excluded to avoid propagation in the radial direction. For $\frac{\lambda_g}{\lambda_o} < 1$ the penetration depth is proportional to this ratio. This penetration plus the radius of the rod should be smaller than the reflecting end plate radius in order to confine the electromagnetic field. It has been found experimentally that in order to obtain the necessary sensitivity a value of λ_g/λ_o of approximately .60 is required. The dielectric constant of the rod, ϵ_d, and the free space wavelength, λ_o, are the two most important parameters determining the radius of the rod, r_o. The radius decreases for decreasing values of the wavelength and increasing values of the dielectric constant of the probe material. It must be emphasized however that these two parameters are not completely independent of the other variables involved in the problem. For instance, the operating wavelength λ_o has to be adopted according to the range of electron densities to be measured. This probe operates with a 3 cm wavelength, corresponding to a critical electron density of approximately 10^{12} e/cm^3. The electron densities to be measured are two orders of magnitude above and below the critical.

The minimum electron density that can be measured depends on the particular technique which is used in measuring the resonant frequency shift of the structure and on the sensitivity of the probe, that is the relative change in resonant frequency referred to a relative change of electron density,

$$S = \frac{\Delta f/f_o}{n/n_c}$$

With an amplitude measurement of the detector output the minimum resonant frequency shift can be taken, as a value, equal to half the bandwidth of the resonance curve when no plasma is present.

$$\left(\frac{\Delta f}{f_o}\right)_{min} = \frac{1}{2\ Q_o}$$

where Q_o is the Q of the structure with no plasma. The sensitivity and the Q must then be chosen so as to have a resonant frequency shift equal to half the bandwidth for an electron density of 10^{10} e/cm^3, i.e.,

$$S = \frac{\frac{1}{2}\ Q}{n_{min}/n_c}$$

or

$$\frac{n_{min}}{n_c} = \frac{1}{2QS}$$

where n_{min} is the minimum measurable electron density.

The upper limit of operation is given primarily by plasma boundary conditions. Near the surface of the probe the electron density departs from that found in the unperturbed region because of charge diffusion and thermal gradients. In this highly overdense condition the penetration depth of the electromagnetic wave has been reduced to a point where it becomes comparable to the thickness of the region of perturbed electron density, and this is taken as the upper limit of measurable electron density. The dielectric material to be used must satisfy several physical requirements. It must be a low loss material in the operating frequency range in order to maximize the Q. The dielectric constant should be within a certain range as discussed below. Machineability is a highly desirable quality. The material should be capable of withstanding high temperatures for as long a period of time as possible and be structurally strong. A number of materials have been investigated for these purposes such as Teflon, lucite, fused alumina and boron nitride. In general boron nitride seems to be more advantageous as far as the above requirements are concerned.

A necessary characteristic of the probe is that it should have only one resonant frequency for each electron density within the total range of operation. This range of resonant frequency shift should be large enough to provide the desired sensitivity. Among all the possible modes which may exist in this structure those differing from the TE family are eliminated by techniques described below, while all TE ;modes, except for the particular one desired, are eliminated through proper choice of the frequency range. The latter is attained through proper selection of probe length, radius and dielectric constant. An optimum range of frequencies can be obtained only if an additional variable is introduced in the design of the probe. This has been achieved by the consideration of a tubular geometry instead of a solid dielectric rod.

It is also possible to build a probe in which the frequency is maintained constant and the effect of the plasma is to alter λ_g, thus producing a phase shift of the standing wave pattern along the rod (Ref. 3). This method of operation would greatly simplify the microwave circuitry associated with the probe. Such a probe consists of a dielectric waveguide with a reflecting surface at one end and a perfectly matched input, for all possible phase shifts, at the other. A detector is used to monitor the position of the minimum voltage of the standing wave pattern, which in turn is related to the electron density of the surrounding plasma. Two difficulties are encountered with this arrangement. The first is that in order to provide a sensitivity comparable with that of the probe already described (variable resonant frequency) the length of the dielectric waveguide must be increased by a factor of five and the phase shift measurement accuracy must be within a half degree. The second difficulty is that of providing a coupling which is matched for all possible phase shifts without exciting undesired electromagnetic modes. Such a coupling must have an input from a rectangular waveguide (TE_{01} mode) and an output to a circular waveguide (TE_{01} mode). The length of a transition such as this is approximately 40 centimeters (Refs. 13 and 14).

A third scheme of operation was investigated in which the probe operates at a constant frequency and the resonance measurement is performed with a tuning element. The electron density is then obtained as a function of a tuning device position. Figure 2 shows a configuration operating according to this idea. The coupling is performed by inserting a portion of the dielectric waveguide in a metallic cylinder. The plane of both input and output loops are located in the azimuthal plane in a region of maximum magnetic field. Two evanescent fields exist in this configuration, the radial one in the plasma-microwave interaction region and the axial inside the metallic cylinder, which is a below cutoff waveguide for the TE_{01} mode. In principle it is possible to compensate for the effect of one of these fields by acting on the other. A resonance is found with no plasma surrounding the probe and with the piston all the way against the dielectric. As the electron density begins to increase the resonant frequency also increases but can be brought down by allowing the axial field to build up, that is by moving the tuning piston. Measurements performed with this instrument show that this principle of operation is feasible. A description of the interaction between radial and axial evanescent fields can be found in Ref. 15, Section III, pages 15-16.

A comparison of the three schemes of operation shows that a resonant frequency shift probe offers a minimum size of the sensing element, together with a reasonable complexity of the associated electronic equipment. The phase shift probe simplifies the microwave circuitry at the expense of a much larger and complex sensing element. Finally the mechanically tuned probe offers a relatively small probe together with simpler associated equipment but with the limitations introduced by the tuning mechanisms. For an inflight application of this probe the variable resonant frequency principle was adopted on the basis of these considerations.

IV. Mathematical Analysis of a Dielectric Rod - Plasma Interaction

A basic description of the principle of operation of the slow phase velocity probe as well as a qualitative description of the variables affecting its design have been presented. A more rigorous mathematical analysis of the dielectric rod-plasma interaction will now be derived by considering the dispersion relation obtained by solving the wave equation in cylindrical coordinates. Considering a circular dielectric waveguide of radius r_o, length z_o, and refractive index κ_d, surrounded by a plasma of refractive index κ_p one finds the dispersion relation for the TE_{01n} mode to be given by

$$\frac{1}{x}\ \frac{J_1(x)}{J_o(x)} = -\ \frac{1}{y}\ \frac{K_1(y)}{K_o(y)}$$

where

$$x = r_o\left(\frac{\omega^2}{c^2}\ \kappa_d^{\ 2} - \frac{n^2\pi^2}{z_o^{\ 2}}\right)^{1/2} \quad ; \quad y = r_o\left(\frac{n^2\pi^2}{z_o^{\ 2}} - \frac{\omega^2}{c^2}\ \kappa_p^{\ 2}\right)^{1/2}$$

J and K are the Bessel function of the first kind and the modified second kind, respectively. No radial propagation occurs as long as

$$\frac{n\pi}{z_o} > \frac{\omega}{c}\ \kappa_p$$

If this condition is satisfied in the range of small electron densities ($\omega_p < \omega$) the dispersion relation yields

$$\mathrm{Re}\left(\frac{\Delta\omega}{\omega_o}\right) \sim K_s \frac{\omega_p^2}{\omega_o^2} \frac{1}{1 + \nu^2/\omega_o^2}$$

$$\Delta\left(\frac{1}{Q}\right) \sim 2 K_s \frac{\omega_p^2}{\omega_o^2} \frac{\nu}{\omega_o} \frac{1}{1 + \nu^2/\omega_o^2}$$

where the sensitivity K_s is given by

$$K_s = \left(1 - \frac{y_o}{x_o} \frac{F'(x_o)}{G'(x_o)}\right)^{-1}$$

ω_o is the resonant frequency without plasma ($\varkappa_p = 1$) and $\mathrm{Re}(\Delta\,\omega/\omega_o)$ is the relative shift of resonant frequency from the lower limit ω_o. x_o and y_o are the values of x and y for $\omega = \omega_o$. The derivatives are

$$F'(x_o) = \frac{d}{dx}\left(\frac{1}{x} \frac{J_1(x)}{J_o(x)}\right)_{x_o} \quad ; \quad G'(y_o) = \frac{d}{dy}\left(\frac{1}{y} \frac{K_1(y)}{K_o(y)}\right)_{y_o}$$

Thus the resonant frequency shift for $\omega_p \ll \omega_o$ is proportional to the electron density of the plasma.

For high electron densities where

$$\frac{\omega_p^2}{\omega^2} \left| \frac{1}{1 - i\ \nu/\omega} \right| > 1$$

the relations for $\mathrm{Re}(\Delta\, \omega/\omega_1)$ and $\Delta\, (1/Q)$ become

$$\mathrm{Re} \left(\frac{\Delta\omega}{\omega_1} \right) \sim -\, K_{s1} \frac{\omega_1}{\omega_p} \sqrt{\left(1 + \frac{\nu^2}{\omega_1^2} \right)^{\frac{1}{2}} + 1}$$

$$\Delta \left(\frac{1}{Q} \right) \sim 2\, K_{s1} \frac{\omega_1}{\omega_p} \sqrt{\left(1 + \frac{\nu^2}{\omega_1^2} \right)^{\frac{1}{2}} - 1}$$

where

$$K_{s1} = \frac{x_1^2\, c^3}{\sqrt{2}\, \omega_1^3\, r_o^3\, \varkappa_d^2}$$

and where x_1 is the first root of $J_1(x) = 0$, and ω_1 is the resonant frequency when the plasma is replaced by a perfect reflecting surface at $r = r_o$. $\mathrm{Re}(\Delta\omega/\omega_1)$ is the relative shift in resonant frequency from the upper limit ω_1. In this case the resonant frequency shift is seen to be inversely proportional to the square root of the electron density.

The minimum electron density that can be measured depends on the particular technique which is used; with an amplitude measurement of the resonant output signal it can be taken to be the value which produces a resonant frequency shift equal to half the bandwidth with no plasma present, i.e.,

$$\left(\frac{\Delta\omega}{\omega_o}\right)_{min} = \frac{1}{2\,Q_o}$$

or

$$\frac{n_{min}}{n_c} = \frac{1}{2\,Q_o\,K_s}$$

where n_c is the critical and n_{min} the minimum measurable electron density. Typical values are $Q_o \sim 10^3$ and $K_s \sim 10^{-1}$, consequently electron densities two orders of magnitude below the critical value can be measured.

The maximum measurable electron density can be defined in an entirely similar manner. The minimum detectable frequency shift is taken as half the bandwidth of the resonant curve with the probe enclosed by an overdense plasma. Denoting the Q in this condition as Q_1 gives

$$\frac{n_{max}}{n_c} \sim 8\,K_{s1}^{\;2}\,Q_1^{\;2}$$

The value of $8\,K_{s1}^{\;2}$ is close to unity, thus n_{max} may be several orders of magnitude higher than n_c with a relatively low value of Q_1. However, other limitations must be considered in this range. Plasma dynamic considerations require that the penetration depth of the electromagnetic wave at the maximum measurable electron density be large compared to the thickness of the layer near the probe where n departs significantly from the unperturbed value. The penetration depth, δ, of an electromagnetic wave inside a strongly overdense plasma is given by

$$\delta \sim \frac{c}{\sqrt{2}\,\omega_p} \sqrt{\left(1 + \nu^2/\omega^2\right)^{\frac{1}{2}} + 1}$$

An estimation of the plasma boundary effects due to charge diffusion and thermal boundary layer indicates that the thickness of the region where the electron density is affected is small enough so that an electron density of approximately 10^{14} e/cm^3 can be measured.

As mentioned before the use of a dielectric tube instead of a rod allows for a better selection of the characteristics of the probe. The considerations made for the behavior of the dielectric rod are also valid for this geometry. The mathematical analysis is performed by solving Maxwell's equations in cylindrical coordinates for three different regions: the central hole, the dielectric material and the plasma surrounding the probe. The boundary conditions at the surface of separation between two media lead to the corresponding dispersion equations. If no losses are considered the fundamental symmetric modes (TE and TM) give the dispersion equations below. For the TE_{01} mode

$$\left[J_o\ (k_1a)\ \frac{I_1(k_2a)}{I_o(k_2a)} - J_1\ (k_1a)\ \frac{k_2}{k_1} \right] \left[\frac{K_1(k_3b)}{K_o(k_3b)}\ N_o\ (k_1b) + \frac{k_3}{k_1}\ N_1(k_1b) \right] =$$

$$\left[N_o(k_1a)\ \frac{I_1(k_2a)}{I_o(k_2a)} - N_1(k_1a)\ \frac{k_2}{k_1} \right] \left[\frac{K_1(k_3b)}{K_o(k_3b)}\ J_o(k_1b) + \frac{k_3}{k_1}\ J_1(k_1b) \right]$$

and for the TM_{01} mode

$$\left[\frac{\kappa_d^2}{\kappa_p^2}\ \frac{k_3}{k_1}\ N_1(k_1b) + \frac{K_1(k_3b)}{K_o(k_3b)}\ N_o(k_1b) \right] \left[\kappa_p^2\ \frac{k_2}{k_1}\ J_1(k_1a) - \frac{I_1(k_2a)}{I_2(k_2a)}\ J_o(k_1a) \right] =$$

$$\left[\kappa_d^2 \frac{k_2}{k_1}\ N_1(k_1a) - \frac{I_1(k_2a)}{I_o(k_2a)}\ Y_o(k_1a) \right] \left[\frac{\kappa_d^2}{\kappa_p^2}\ \frac{k_3}{k_1}\ J_1(k_1b) + \frac{K_1(k_3b)}{K_o(k_3b)}\ J_o(k_1b) \right]$$

where

$$k_1 = (\kappa_d^2 k_o^{\ 2} - k_z^{\ 2})^{\frac{1}{2}}$$

$$k_2 = (k_z^{\ 2} - k_o^{\ 2})^{\frac{1}{2}}$$

$$k_3 = (k_z^{\ 2} - \kappa_p^2 k_o^{\ 2})^{\frac{1}{2}}$$

and where J and N are Bessel functions of the first and second kind, respectively, I and K are modified Bessel functions of the first and second kind, respectively, κ_d is the refractive index of the dielectric material, κ_p is the refractive index of the plasma, $k_o = \omega\sqrt{\epsilon_o \mu_o}$, $k_z = \frac{n\pi}{z_o}$, and where a and b are the inner and outer radii of the tube, and z_o is the length.

A numerical computation (Ref. 15) has been performed for a typical probe in order to show the relation between electron density and resonant frequency shift for a TE_{01} mode of operation. The result of this computation is shown in Fig. 3. The magnitude of the electric and magnetic fields has been computed for the same probe. The resulting equations for the different regions of the probe are

$$E = \begin{bmatrix} 0 \\ \dfrac{k_o^2}{i\omega\epsilon_o} \dfrac{I_1(k_2 r)}{k_2} \sin k_z z \\ 0 \end{bmatrix} \qquad (0 < r < a)$$

$$E = \begin{bmatrix} 0 \\ \dfrac{k_o^2}{i\omega\epsilon_c} \dfrac{[D_1 J_1(k_1 r) + D_2 N_1(k_1 r)]}{k_1} \sin k_z z \\ 0 \end{bmatrix} \qquad (a < r < b)$$

$$E = \begin{bmatrix} 0 \\ -\dfrac{k_o^2}{i\omega\epsilon_o} \dfrac{G\ K_1(k_3 r)}{k_3} \sin k_z z \\ 0 \end{bmatrix} \qquad (b < r)$$

$$H = \begin{bmatrix} -\dfrac{k_z I_1(k_2 r)}{k_2} \cos k_z z \\ 0 \\ I_o(k_2 r) \sin k_z z \end{bmatrix} \qquad (0 < r < a)$$

$$H = \begin{bmatrix} -\dfrac{k_z[D_1 J_1(k_1 r) + D_2 N_1(k_1 r)]}{k_1} \cos k_z z \\ 0 \\ [D_1 J_o(k_1 r) + D_2 N_o(k_1 r)] \sin k_z z \end{bmatrix} \qquad (a < r < b)$$

$$H = \begin{bmatrix} \dfrac{k_z G\ K_1\ (k_3 r)}{k_3} \cos k_z z \\ 0 \\ G\ K_o(k_3 r) \sin k_z z \end{bmatrix} \qquad (b < r)$$

where

$$D_1 = \frac{\pi a k_1}{2} \left[\frac{k_1}{k_2} I_1(k_2 a) J_o(k_1 a) - I_o(k_2 a) J_1(k_1 a)\right]$$

$$D_2 = \frac{\pi a k_1}{2} \left[I_o(k_2 a) N_1(k_1 a) - \frac{k_1}{k_2} I_1(k_2 a)\ N_o(k_1 a)\right]$$

$$G = \frac{D_1 J_o(k_1 b) + D_2 N_o(k_1 b)}{K_o(k_3 b)}$$

and where the other parameters are identical to those given previously.

Figures 4 and 5 show the magnitudes of these fields, where the axial magnetic field at the tube center has been taken as one ampere per meter. The configuration of the radial magnetic field is identical to the azimuthal electric field. The curves are shown for three values of ambient electron density: $n/n_c = 10^{-2}$, 1, and 10^2.

V. Electromagnetic Coupling for the Dielectric Probe

The dielectric probe is made to operate as a transmission resonant structure such that the microwave generator is able to deliver power to the detector only in the vicinity of the resonant frequency. Several coupling configurations have been studied to determine the most convenient circuit for both input and output. Desirable properties of such a coupling are mode discrimination enhancing the desired TE_{01n} mode over the frequency range of operation, and a large output for the values of Q of the probe in the operating frequency range.

The two basic types of coupling are loops terminating coaxial lines and holes in waveguides adjacent to the resonant structure.

Figure 6a shows a coupling performed with waveguides. An E-plane tee (also called a series tee) has the property that the electric field at the input propagates with opposite phases in both arms and that the power is divided equally between the two arms if the loads are equal. For the construction shown here the loads are short circuits symmetric with respect to the input. The standing wave generated preserves the symmetry of the magnetic field, and the holes located at $\lambda_g/4$ from the short circuit excite a radial magnetic field in the probe. For a small size of the holes no electric field is excited. An entirely similar device is located at the other end of the dielectric tube. This construction allows for a high symmetry in the excitation, and no electric field is introduced. The main disadvantages are the bulk of the construction and the difficulty of locating both input and output on the same side of the probe. It was also found that a TM_{21} mode is excited, and that in order to eliminate its detection the output should be mounted with a 45° azimuthal shift with respect to the input.

Figure 6b shows a coupling performed with a family of loops located at the plane of the reflector near the center of the dielectric waveguide. The input is a coaxial cable which is split into four loops located in the azimuthal plane. The magnetic field so generated has no azimuthal components. The detector is connected to a similar arrangement at the other end of the dielectric tube. The coupling is not performed in the region of maximum magnetic field corresponding to TE_{01} mode; consequently the size of the loop has to be increased up to a point where it becomes comparable to the wavelength. The electric field along the loop now becomes important and undesired modes are excited.

Figure 6c shows a coupling arrangement where a metallic rod is located along the center of the dielectric tubing. This rod is the shield of a coaxial line. The coupling is performed with helical slots in the shield; the current flowing axially is deviated in correspondence to those slots thus introducing longitudinal components of magnetic field. The coupling region is located $\lambda_g/4$ from the reflector, and the coaxial feeding line is short circuited $\lambda_g/2$ from the slots in order to have a maximum current flowing through the coupling. The output is obtained from a similar circuit mounted at the other end of the dielectric tubing. This coupling allows for a mechanically strong structure and can be adapted so as to have both input and output in the same side. The main problem is that a coaxial family of modes is introduced.

Another coupling performed with loops is shown in Fig. 7. Their location corresponds to the maximum radial magnetic field, consequently their size can be made much smaller than in case 6b. The detector is located at the other side of the dielectric tubing. The behavior of this coupling system was found to be satisfactory. A modified form of this coupling was used in the last version of the probe.

The coupling used in the final version of the probe is shown in Fig. 8. The dimensions have been reduced to a minimum and both input and output are on the same side of the probe. Instead of circular holes a set of four dumbbell couplings are located in one of the reflecting surfaces. For a given linear dimension the dumbbell allows for a stronger coupling and a weaker electric field excitation compared to a circular hole. The coupling is made by a wire which runs perpendicular to the slot of the dumbbell, and in close proximity to it, generating a current and a magnetic field similar to those existing in a strip line. The magnetic field can be maximized by putting a short circuit at a distance equal to $\lambda/2$ from the coupling, or an open circuit at $\lambda/4$.

The connection between coupling holes and external circuits is performed with a double coaxial line where three concentric conductors are used. The inner conductor, "a," feeds two opposite holes exciting in phase radial magnetic fields. The end of the wire is an open circuit at $\lambda/4$ from the coupling. Both signals are added in a "tee" at the axis of the probe and go out to the "A" connector. The intermediate conductor, "b," a tube, couples the other pair of holes which are located at $\lambda/2$ from a short circuit. Here also a tee is used to add the two signals in a symmetric way. The output connector "B" uses a $\lambda/4$ stub to avoid short circuiting the signal while allowing the inner conductor "a" to go out to connector "A."

The relative position of the wires is maintained with teflon spacers, while a brass box with partitions avoids all direct coupling between the two signals, so that the only coupling between input and output is that through the dielectric tube in a resonant condition. The connectors are interchangeable, except that "B" provides a D.C. return to ground while "A" does not. This coupling scheme eliminates the dipole mode which appears with nonsymmetric excitations.

The TM_{21} type mode may appear with this coupling, however it is easily eliminated with a set of six longitudinal wires, as shown in Fig. 8.

VI. The Final Probe and the Calibration With Simulated Plasmas

The final model of the electron density probe consists principally of three sections, the electromagnetic coupling, the dielectric element, and the reflecting plates as shown in Fig. 9. The coupling, as described in Chapter V and seen in Fig. 8, excites the TE_{01} mode. The dielectric element is a boron nitride tube of relative dielectric constant four which has an outer diameter of one inch (2.54 cm), an inner diameter of three eighths of one inch (0.95 cm), and a length of 0.717 inches (1.94 cm). This length corresponds to one full wavelength of the TE_{01} mode in the axial direction. The circular reflectors which terminate the element are one and one half inches in diameter (3.81 cm). This dimension was found to be the minimum which could be taken without seriously affecting the open cavity Q. The resonant frequency of the structure without plasma is 9175 MHz with a corresponding Q of 1500. The upper limit, found by tightly wrapping the element with a metal cylinder is 10,120 MHz with a Q of 1000. This gives a total range of operating frequencies of 945 MHz.

The slow phase velocity probe has been calibrated in the upper and lower portions of the measurable electron density range with plasma simulating materials. In the lowest range of electron densities the plasma has been simulated with a low dielectric constant plastic foam (Ref. 4) which, except for a sign, simulates the perturbation to the electric field produced by a strongly underdense plasma. In the upper range the simulation is performed by wrapping the probe with metallic cylinders of inner radius slightly larger than the outer radius of the probe. The small gap between the two is then related to an equivalent penetration of depth the electromagnetic wave into the plasma. A calibration is made with those devices by precisely determining their equivalent electron densities and measuring the corresponding resonant frequency of the probe.

The equivalent electron density of the dielectric foam is

$$n = (\epsilon_r - 1)\, n_c = (3.36\text{x}10^{-2})\, n_c$$

As the critical electron density n_c for this probe is $1.04\text{x}10^{12}$ e/cm^3 the corresponding electron density simulated by the plastic foam is $3.49\text{x}10^{10}$ e/cm^3. The resonant frequency shift due to this foam was found to be 5.5 MHz. The half bandwidth of the probe response with no plasma is 2.5 MHz so that the linear approximation for the frequency shift, which is valid in this region and which takes the half bandwidth as the lowest detectable shift, gives a minimum detectable electron density of 1.84×10^{10} e/cm^3. The calibration performed with the dielectric foam is shown in Fig. 10.

In the upper range of electron densities the calibration is performed with a metallic cylinder placed coaxial to the probe. The equivalent electron density can be found by determining analytically the resonant frequency shift for such a configuration and comparing it with that found for a highly overdense plasma, as in Chapter IV. For a configuration such as that shown in Fig. 11 the resonant frequency shift is found (see Appendix I) to be

$$\frac{\Delta\omega}{\omega_1} = - \frac{x_1^{\,2} c^2 \Delta r}{\omega_1^{\,2} r_o^{\,3} \varkappa_d^{\,2}}$$

where ω_1 is the resonant frequency as the gap $\Delta r = r_1 - r_o$ approaches zero, x_1 is the first root of $J_1(x)$, and $\varkappa_d$ is the refractive index of the dielectric material. It was found in Chapter IV that with a highly overdense lossless plasma the resonant frequency shift is given by

$$\frac{\Delta \omega}{\omega_1} = - K_{s_1} \frac{\omega_1}{\omega_p} = - \frac{x_1^2 c^3}{\omega_1^2 r_o^3 x_d^2 \omega_p}$$

Comparing these results it is seen that for a given $\Delta\omega$ there is a unique correlation between Δr and ω_p which is given by

$$\Delta r = \frac{c}{\omega_p}$$

where ω_p is angular plasma frequency.

A calibration of the probe has been made utilizing this equivalency. The probe was surrounded by metallic cylinders of varying sizes and the resonant frequency for each noted. An equivalent electron density was then obtained from the last relation. The calibration points obtained in this manner are shown in Fig. 12.

As there is always some degree of direct coupling in such a structure the output of the probe has been measured throughout the entire range of operating frequencies for two conditions. These are the limits of operation, that is no plasma on one hand and tightly wrapped with a metal cylinder of gap $\Delta r = 0$ on the other. The results of these measurements are shown in Figs. 13 and 14. The relative output of resonance is shown throughout the range of operating frequencies in Fig. 15. It is seen that the output is fairly constant throughout the range, varying only by a factor of three.

VII. Calibration with Shock and Discharge Produced Plasmas

A calculation has been made of the plasma conditions in which the probe being developed will be immersed during reentry (see Chapter II). It is important that the plasma used to calibrate the probe be as similar as possible to the above-mentioned reentry plasma with respect to the properties important to the operation of the probe, namely, electron density and collision frequency. Two laboratory plasmas which are capable of producing these properties in a no-flow condition are those found in the reflected shock region of a shock tube and the after-glow region of an arc-discharge tube. Both of these have been used to calibrate the probe. The two gases being used to simulate these conditions in the laboratory are air and argon, each of which offer certain advantages and disadvantages. It was found both analytically and experimentally that for the conditions available in the GASL laboratory facilities, argon offers an important advantage over air. In simulating the proper electron densities with both gases the collision frequency is found to be much nearer the desired value in argon than in air. For this reason studies have been directed towards argon; however, both gases have been used extensively. It should also be noted that the higher collision frequencies found in air not only hampers the operation of the probe but also that of the calibrating interferometers. Two microwave interferometers, operating with 1 cm and 4 mm wavelengths, have been used in this study. The basic characteristics of the two are a maximum measurable electron density of 10^{13} and 7×10^{13} e/cm^3, respectively, and a minimum measurable electron density (ten degree phase shift) of 4×10^{10} and 10^{11} e/cm^3 respectively, when mounted in the shock tube. Typical calibration charts of these two systems are shown in Fig. 16, and a schematic diagram is shown in Fig. 17.

In these interferometers, an interacting signal passes through the plasma and is compared with a reference signal. The effect of the plasma is to cause a phase shift and an attenuation of the interacting signal. This phase shift produces timewise oscillations in the detector output. A typical interferometer trace for a plasma whose electron density increases to a maximum and then decreases again (such as that produced in the incident shock region of a shock tube), will appear as a phase shift of several degrees (or cycles) until the maximum is reached, and then reverses itself and retraces this shift in the opposite direction. As the electron density is increased the interacting signal reaching the detector will be reduced due to partial absorption.

As a consequence the observed traces show an attenuation of the oscillations near the reversal point. This description is for the case of low collision frequency, i.e., $\nu/\omega \sim 10^{-2}$. For larger values the attenuation is greatly increased thus restricting the use of the interferometer. As an example, with $n/n_c \sim 0.5$ the signal of the 1 cm interferometer is reduced by ~ 90% for $\nu/\omega \sim 10^{-1}$, while the reduction is ~ 25% for $\nu/\omega \sim 10^{-2}$. For a plasma whose electron density does not increase monotonically to a maximum and then decrease monotonically to zero this simple approach is not possible. This description further assumes, among other considerations, that the gradient of electron density in the interaction region be small enough so as to provide a meaningful average.

The first facility to be used in the actual calibration of the probe was the shock tube. It was felt that before a meaningful diagnosis of the reflected shock region could be made the incident shock plasma would have to be thoroughly understood. As the delivery of the 4 mm wavelength klystron was delayed several months the investigations were begun with the 1 cm interferometer. A typical study is shown in Fig. 18 for an incident argon plasma. Three traces are shown for various initial (driven) pressures of argon at approximately equivalent Mach numbers. The upper trace in each is that of the (one cm wavelength) interferometer, while the lower is a marker. Fig. 3, for instance, yields values for collision frequency and electron density at peak conditions behind the incident shock of approximately $2x10^8$/sec and $2x10^{12}$ e/cm^3, respectively. The corresponding equilibrium values are approximately $2x10^8$/sec and $3x10^{14}$ e/cm^3, respectively. The discrepancy in electron density has been noted previously in the literature (Refs. 16, 17, 18, and 19). The duration of the plasma has been estimated from these three traces (Fig. 18) and plotted in Fig. 19. This time has been arbitrarily taken as that during which a detectable phase shift appears in the corresponding interferometer trace. Again, similar findings have been noted in the literature (Ref.20). With the arrival of the 4 mm klystron the second interferometer was used to check the conditions corresponding to Fig. 18b. The trace obtained is shown in Fig. 20, where it is seen (upper trace) that this also gives a peak electron density of approximately $2x10^{12}$ e/cm^3. Similar traces for incident air plasmas are not as easily analyzed because the much increased collision frequency causes a far greater attenuation of the observed oscillations (Refs. 21 and 22).

Having what was considered to be a sufficient understanding of incident shock plasmas, a study was begun of the reflected shock region. This again was begun with the 1 cm interferometer and then continued with the 4 mm interferometer when available. Studies were made for several conditions in which the position of the reflecting plate was varied systematically between two positions. This plate represented the end of the shock tube as far as the flow was concerned, or more specifically, it was in this region that the reflected plasma was to be found. The two positions were (a) well downstream of the interferometer and (b) adjacent to the downstream edge of the interferometer horn. In this way it was possible to obtain the trace due to the incident plasma alone, and then to subtract this from the trace obtained in the reflected shock region. It is then possible to successfully separate the trace due to the reflected shock and analyze it apart from the rest. Even with this technique, it is extremely difficult, if not impossible, to draw significant conclusions concerning the properties of the reflected region plasma. This is due primarily to the failure of the reflected shock region plasma to meet two requirements mentioned earlier; first that the plasma be sufficiently uniform in the region of interaction and second, that the electron density increase and decrease monotonically. In addition, it is found that the reflected plasma is smaller in length and lower in electron density than that anticipated (Ref.23). Fig. 21 shows the trace obtained with the 4 mm interferometer with an endplate adjacent to the horn. The left part of the trace corresponds to the incident plasma and it can be analyzed in terms of the phase shift. The part at the right shows the effect of the reflected shock which is very difficult to analyze.

Two techniques were developed to overcome the difficulty of properly diagnosing this reflected shock region plasma. The first was to produce a weaker plasma such that the interferometer trace was just a 180° phase shift (one-half cycle). In this experiment the phase shifter on the interferometer is set so that the signal begins either in the minimum or maximum. The highest electron density attained in the reflected region then deflects the output signal to a 180° shift (to the opposite extreme) and 180° back, giving the appearance of a full cycle. If the highest electron density attained is less than the required value the amplitude of the observed deflection will be smaller than that anticipated, while if it is higher some uninterpretable fluctuations will begin to appear at the reversal point of the interferometer trace. With this technique at least one point can be found where the electron density is known in the reflected shock region. With the 4 mm interferometer horns mounted flush to the wall of the shock tube the electron density corresponding to a maximum deflection of a half cycle of $1.6\text{x}10^{12}$ e/cm^3. The probe is then inserted in the test section exactly where the interferometer measurement was made and the flow parameters exactly reproduced. A study is then made to find the greatest frequency for which the probe will react. It is then concluded that this frequency corresponds to the value found with the interferometer. This particular technique has been used for two geometries as shown in Fig. 22. Part (a) shows the position of the probe support and first reflector, with the interferometer horns looking through the region where the probe element and second reflector will later be placed. After determining the flow conditions which produce a half cycle in the interferometer trace, the horns are replaced by the probe as shown in (b). Part (c) shows the same arrangement as in (a) except that now a screen is placed in front of the probe holder. The conditions needed to produce a half cycle interferometer trace in this configuration are not the same as for the first so that the entire procedure must be repeated. As before the probe element (dielectric waveguide) then replaces the interferometer horns. The two calibration points obtained in this manner are shown in Fig. 12. The first configuration gave a maximum frequency shift of 100 MHz while the second gave a shift of 90 MHz. It is worthwhile pointing out that although the calibration of the probe could not be extended beyond the two points obtained, a resonance of the probe has been detected throughout the entire range of operating frequencies in the configuration of Fig. 22b. Fig. 23 shows the reaction of the probe at a frequency shift of 700 MHz which according to the calibration performed with the metallic cylinders corresponds to an electron density of 5×10^{13} e/cm^3.

The second attempt to overcome the difficulties of diagnosing the reflected shock plasma consisted essentially of replacing one of the interferometer horns by a reflecting mirror as shown in Fig. 24b. The reflecting mirror of this double-path interferometer was then placed at a distance equal to the length of the boron nitride probe ahead of the horn in a direction coaxial with the shock tube, as shown in Fig. 24a. In this way the probe could be placed in the same configuration and then calibrated with the results obtained from the interferometer. An interferometer trace obtained for this arrangement is shown in Fig. 25. It is seen here that the interpretation of the obtained trace is not straightforward. For this reason no attempts were made to calibrate the probe in this condition A measurement such as that described above utilizing the half cycle reversal point might have been possible for this configuration but it was not fully investigated because of a lack of time.

The second facility to be used for the probe calibration was a discharge tube in which simultaneous measurements of electron density were made with the 4 mm interferometer and the probe in the afterglow region. A schematic diagram of the facility is shown in Fig. 26. The plasma is obtained by discharging a 90 MF capacitor (with a 6 KV maximum rated voltage) through two 15 cm diameter disks at a separation distance of 65 cm. The glass test section surrounding the disks has four ports located in the center such that they face each other in pairs, with the respective pair axes separated by 5 cm. With this arrangement the interferometer horns were mounted through one pair, flush to the tube wall, while the probe was inserted through one of the remaining ports. Using argon the discharge is produced at a reduced pressure and outputs are monitored from both devices. As the electron density decreases time-wise in the afterglow region an output of the probe will be observed. The calibration is then made by associating the preset frequency shift of the probe with the electron density measured with the interferometer at the time when a resonance is observed in the probe. A typical trace is shown in Fig. 27. In this picture the probe is set at a frequency of 125 MHz above the resonant frequency with no plasma. The output is seen (lower trace) to occur at a time when the interferometer reads (for this horn separation)

2.1×10^{12} e/cm^3. The calibration points obtained in this manner are shown in Fig. 12. These points were obtained at an initial pressure of .035 mm Hg argon and a potential of 500 volts. The 1 cm and 4 mm interferometers were used simultaneously in order to check the obtained traces. It was found that the two saw the same electron density. A typical trace comparing the two is shown in Fig. 28. In these conditions the calibration of the probe was performed in the range of electron densities from 4×10^{10} to 1×10^{13} e/cm^3. The upper limit of electron density in the calibration process mentioned above is limited by the high noise level of the recorded signal at small time intervals immediately after the end of the discharge current. To increase the upper limit of this calibration a stronger discharge is required. However, for stronger discharges it was observed that the time correlation between the resonance of the probe at a given frequency and the interferometer reading depends upon the applied voltage, namely the discharge strength. This situation made it impossible to use the discharge induced plasma for the probe calibration in the upper range of measurable electron densities.

A final resonant frequency shift vs. electron density curve has been constructed utilizing the calibration points obtained with both the real and simulated plasmas described. The curve is shown by the solid line in Fig. 12. The lower portion of the curve, in the range 10^{10} to 10^{11} e/cm^3 was determined primarily by the dielectric foam calibration and the knowledge that the resonant frequency is linearly related to the electron density in this range. The middle portion of the curve, corresponding to 10^{11} to 10^{13} e/cm^3, has been determined primarily on the calibrations performed with the shock tube and electrical discharge produced plasmas. The remaining section of the curve was determined primarily on the basis of the calibration performed with the metal cylinders. An inspection of the curve shows that in general these portions overlap each other. For the purpose of illustration the approximations for small electron densities and for highly overdense plasmas (see Chapter IV) have been shown.

VIII. Estimated Perturbation of the Electron Density Distribution Due to Diffusion and Heat Transfer

Due to the physical presence of the probe in the ionized gas the measured electron density may differ from that in the unperturbed gas. These perturbations arise from locally induced changes in flow field properties due to local transport phenomena and the geometry of body. Ideally the probe is to be located in the zero velocity region of the separated flow. However one must expect that during the inflight application finite velocity gradients will exist near the probe. For a location 75 cm aft of the shoulder it is estimated that the velocities about the probe should not exceed 100 m/sec for a flight condition with a velocity of 33 kfps and an altitude of 200 kft. This situation corresspons to the first penetration to an altitude of 200 kft for the 3000 nm reentry trajectory with a reentry angle of -6.4°. Peak electron densities and heat transfers are estimated to occur in the vicinity of this flight condition. Further, since temperatures in this region are estimated to be about 5400° K the corresponding Mach number will be about 0.1. Therefore locally induced changes in density due to flow perturbations will be small.

Under the aforementioned flight conditions the electron density distribution surrounding the probe should be primarily affected by heat transfer from the gas to the relatively cold probe surface and the diffusion process of the charged particles toward the probe.

The assessment of the heat transfer effects on the local electron density is quite difficult for a number of reasons. First, it is well known that the description of the fluid mechanics of the flow in the separation region is incomplete. Only the gross flow field properties are qualitatively understood and both detailed experimental and analytical investigations of the flow in these regions are not yet available. Further discussions of the environment anticipated can be found in Chapter X. Furthermore the altitude range over which the probe is to operate results in local flow regimes extending from continuum flow at 150,000 ft to free molecular flow at 350,000 ft. Finally as mentioned previously velocity gradients exist in the separated flow region which preclude consideration of purely conductive heat transfer from the air to the probe. Estimates of the local flow properties for the 200,000 ft altitude case where a local velocity of 100 m/sec was taken, indicate that Reynolds number based on the probe diameter is about 5. The estimated mean free path is 0.28 mm with a corresponding Knudsen number of about 0.01. This flight condition at 200,000 ft then appears to present local flow conditions which are on the borderline between continuum flow and slip flow. Furthermore the Reynolds number of 5 indicates that a Stokes like flow condition will prevail around the probe. This flight condition then represents a flow situation for which heat transfer effects could be estimated and be used as a base from which departures into either more well established continuum or rarefied flow regimes could be assessed. The fact that the surface temperature of the probe is relatively cold compared to the ambient temperature makes it impossible to apply existing incompressible Stokes flow solutions about the cylindrical sensitive element of the probe. Further there does not appear to be any available theoretical treatment of this problem. Numerical solutions of the flow around cylinders in low density flow using Monte Carlo techniques have been published in Ref. 24 however the calculations have been restricted to Knudsen numbers above 0.10 because of computing machine capacity limitations. Therefore in order to obtain an estimate of the temperature gradient above the surface of the probe use has been made of the available experimental heat transfer data obtained for cylinders in flow situations comparable to those of interest here. The heat transfer data used is presented in Ref. 25 where the Nusselt number is given as a function of Reynolds number.

These data were used to determine the heat flux to the probe wall in the following manner. The heat transfer coefficient h is obtained from the relation

$$h = N_N \cdot \frac{k_t}{D}$$

where N_N is the Nusselt number obtained from Ref. 25, k_t is the air thermal conductivity at the total air temperature and D is the diameter of the probe. The temperature gradient at the wall is obtained from the relation

$$h\ (T_w - T_o) = -\ k_w \left(\frac{dT}{dy}\right)_w$$

where T_w is the wall temperature, T_o is the recovery temperature (for the Mach number under consideration here the recovery temperature is equal to the total temperature, Ref. 26), k_w is the thermal conductivity at the wall temperature and $(dT/dy)_w$ is the temperature gradient at the wall. For the 200,000 ft altitude conditions mentioned above (Reynolds number = 5, Mach number = 0.1) the temperature gradient at the wall is calculated to be 0.7×10^4 °K/mm.

These results are indicative of large temperature gradients and that the asymptotic temperature is reached within a distance of the same order as the penetration depth of the electromagnetic field in a plasma with an electron density $\leq 10^{14}$ e/cc. Even assuming that the local value of the electron density corresponds to thermal and chemical equilibrium everywhere there should be no significant perturbation of the electron density measurement due to heat transfer at this flight condition. As was pointed out before this 200,000 ft altitude flight condition has associated with it estimated vehicle separated local flow conditions which are in the transition region between continuum and slip flow. Above 200,000 ft rarefied gas effects will exist in the local flow around the probe. In particular in the upper range 300-350 kft locally a free molecular flow will exist around the probe. The mean free path is comparable to the probe dimensions and it is meaningless to compute a temperature gradient. Furthermore, in this regime the charged particles will interact with the surface of the probe independently of the neutral particle distribution around the probe. As a consequence heat transfer considerations in the upper range of altitude should be even less significant than those estimated for the 200,000 ft case. Since heat transfer effects do not appear to be significant at both ends of the range from 200 kft to 350 kft it is not expected that substantial perturbations in electron densities due to heat transfer effectswill arise at intermediate altitudes. At altitudes lower than 200 kft one can expect departures from Stokes like flow and although calculated temperature gradients will be larger than those determined for 200 kft there will be an onset of vortex sheding which will result in unsymmetrical flow distributions about the probe. Estimates of the heat transfer and local flow effects are difficult and the probe operation should be checked experimentally under these conditions. However before an effort is made in this direction it is recommended that a careful study of the effects of ablation products on the electron density level be made because preliminary estimates of the electron density in the separated flow region for pure air chemistry at 150,000 ft indicates that the electron density is below the lower limit of operation of the probe.

An additional perturbation of the electron density distribution due to the physical presence of the probe in the ionized gas is caused by the diffusion of charged particles (ions and electrons) towards the surface of the probe.

The effect of the diffusion processes is to decrease the electron density at the wall of the probe compared to the electron density in the unperturbed medium. A gradient of electron density is found at the surface of the probe in a direction perpendicular to the surface itself. Therefore the error introduced in the measurement is small only if the electron density gradient at the probe surface is sufficiently large such that the electron density attains a value close to the unperturbed value within the penetration depth of the electromagnetic field of the probe inside the plasma.

At altitudes where a continuum approach to this problem can be used for the range of electron densities of interest, one may assume that the electrons diffuse toward the surface of the probe according to the ambipolar diffusion model.

To estimate the order of magnitude of the diffusion effect one can consider the axisymmetric problem of a cylinder of infinite length where the diffusion occurs only in the radial direction. In the range of temperatures up to 5000° K the ionization reaction

$$N + O + 2.8 \text{ ev} \rightleftarrows NO^{+} + e^{-} \qquad (1)$$

can be considered the dominant one. In this particular case the ambipolar diffusion in the radial direction in the ionized gas surrounding the cylinder is governed by the equation

$$\frac{d^2 y}{dr^2} + \frac{1}{r}\frac{dy}{dr} = \alpha^2 \; (y^2 - 1) \qquad (2)$$

where $y = n/n_\infty$, n is the local value of electron density and n_∞ is the value of electron density in the unperturbed medium, i.e. at $r \to \infty$.

The constant α is given by

$$\alpha^2 = \frac{k_D \; n_N \; n_O}{D \; n_\infty}$$

where n_N, n_O are the nitrogen and oxygen number densities, respectively. k_D is the forward reaction rate of Eq. (1). D is the ambipolar diffusion coefficient.

Eq. (2) must be solved numerically and, as a boundary condition at the surface of the cylinder ($r = r_o$) one can assume a value of the electron density which is negligible compared to n_∞. With this assumption one overestimates the effect of the diffusion process. The numerical integration of Eq. (2) is presented in Fig. 29 for several values of α^2. One observes that the effect of the diffusion is substantial for $\alpha^2 < 1 \text{ cm}^{-2}$.

For the assigned trajectory when the altitude falls below 200 kft the value of α^2 is found to be larger than 1 cm^{-2}. On the other hand as the altitude falls below 200 kft during the final part of the reentry the expected electron density in the unperturbed medium should be small and even below the range of operation of the probe. In any event no substantial perturbation due to the diffusion process has to be expected in the altitude range between 200 kft and 150 kft. During the initial phase of the reentry at the minimum altitude of 200 kft (90 seconds in Fig. 1) the computed value of α^2 is in the range between 1-10 cm^{-2}.

At 200 kft the mean free path for the neutral particle is .28 mm as indicated before and the continuum approach is still valid. At higher altitudes where the mean free path is of the order of the penetration depth of the electromagnetic field a continuum theory is not valid and Eq. (2) cannot be used to compute the electron density profile around the cylinder. In the upper range of altitudes which correspond to a mean free path of the order or larger than the diameter of the cylinder it is expected that the Debye shielding distance be the dominant parameter in defining the extent of the perturbation in electron densities around the probe. Even for the lowest value of measurable electron densities $n_e = 10^{10}\ e/cm^3$ the Debye shielding distance is $\sim 5 \cdot 10^{-3}$ cm. Therefore in view of the extremely small value of the Debye shielding distance for the operating range of the probe compared to the penetration depth of the electromagnetic field in the plasma one should not expect a significant error in the measurement.

IX. Manual of Operation

The equivalent circuit of the probe is shown in Fig. 30a. This corresponds to a transmission cavity whose resonant frequency is a function of the plasma electron density interacting with the electromagnetic field attached to the dielectric rod. Two couplings, "A" and "B," are furnished, both with under critical coupling. Energy between the two connectors can be transmitted at resonance only. If a microwave generator is connected to "A" and a microwave detector to "B," only one value of electron density will allow the signal to reach the detector for a given setting of the input frequency. There is, therefore, a unique correspondence between electron density and resonant frequency throughout the specified range of operating frequencies.

Either connector "A" or "B" can be used as an input, or output, but it is worthwhile noting that "A" does not provide a D.C. return, as required for most microwave detectors. This characteristic is shown by including a fictitious condenser, "C," in the equivalent circuit. A variety of methods can be used to detect the resonant condition of the probe. The circuit and procedure presented here correspond to that employed during the calibration of the probe. The layout is shown in Fig. 30b. A klystron power supply (FXR Z3198) feeds a 3 cm wavelength klystron (Sperry 2K39). The klystron output goes through an isolator (Airtron 332170), a wave meter (Sperry 12X1), an attenuator (DeMornay-Bonardi DBG-915), and a directional coupler (DeMornay-Bonardi B1). The power supply allows continuous wave operation as well as several types of modulation. The directional coupler furnishes a reference for checking the power and frequency of the generated signal. The output of the microwave system is fed to the probe input "A." Connector "B" is used to feed a crystal detector (1N76) whose output is displayed on a double beam oscilloscope (Tektronix type 551, Type D preamplifier) together with the reference.

A photographic camera can be used as an information recording device when the probe is used simultaneously with an interferometer. Both signals can be displayed in one oscilloscope thus simplifying any desired comparisons. An appropriate circuit has to be used to trigger the oscilloscope trace. For the calibration of the probe in a shock tube, heat transfer gages were used as triggers, while in an electrical discharge the sweep was initiated with a signal obtained from a current sensing coil.

The following steps indicate a systematic approach for the measurement of electron densities with this probe.

1. Determine the resonant frequency of the probe without plasma. This is done by varying the frequency of the microwave generator until an output from the probe is found. the wavemeter can then be used to determine this frequency, f_o, which should be the same as that indicated on the calibration chart (Fig. 31). By using a pulse modulated signal the rise time of the detecting circuit can be determined. To obtain a resolution on the order of several microseconds it may be convenient to connect a resistance in parallel with the crystal to compensate for any capacities introduced.

2. After estimating the expected electron density, the corresponding frequency shift, Δf, can be found from Fig. 31. The microwave generator is then set at a frequency equal to $f_o + \Delta f$. As the output signal of the detector varies over wide limits, depending on its own characteristics as well as that of the plasma and the microwave generator, the required pre-amplifier sensitivity to be used can only be found by performing the measurement. During the calibration of the probe outputs between 100 mv and 1 mv were obtained. The sweep speed of the oscilloscope must be

chosen according to the expected duration of the plasma under study. The shock or discharge should now be initiated and the resulting photographic trace interpreted. The main consideration at this point would be to determine whether the electron density to be measured is above or below that for which the probe has been set. In a shock tube, for instance, where the electron density behind the incident shock first builds up and then decays after reaching a maximum, one will find no probe output if the preset frequency corresponds to an electron density higher than the maximum obtained, one output if they are just equal, and two outputs if the preset value is lower. The oscilloscope setting (time and amplitude) should now be reset to optimize the obtained photographs. In the electrical discharge the building up time of electron density is very short and is marked by strong interference due to the high currents in the circuit. Consequently the measurement is performed only in the afterflow region. In this situation the reaction of the probe moves towards the time origin as Δf is increased, to a point where it becomes indistinguisable from the interference introduced by the discharge.

The probe output will be seen to decrease with increasing electron collision frequency for a given preset condition. This is most easily observed in the reflected region of a shock tube where the response to the incident plasma will in general be greater than that of the reflected plasma for the same preset frequency.

X. In Flight Application of the Probe

A. Separated Flow Patterns

The separated flow patterns about the afterbody of the Apollo spacecraft is to a large extent unknown. While numerous studies have been made of the heat transfer to the afterbody surface little has been done to determine the details of the flow within the separated flow region. In Ref. 27 results were reported on measurements of the boundaries of the separated flow over the afterbody for 0° and 35° angle of attack. These results indicate that when one considers the leeward side of the vehicle the inclination of the separated flow boundary remains essentially fixed with respect to the velocity vector of the spacecraft as the angle of attack is varied from 0° to 35°. Based on this information from Ref. 27 it is possible to estimate roughly the boundary of the separated flow region for a 20° angle of attack which was used herein as the design angle of attack for the problem of sizing the length of the probe support.

The separated flow boundary on the leeward side for a 20° angle of attack can be roughly defined by a line in the pitch plane extending rearward from the front heat shield shoulder at an angle of 40° with respect to the surface of the afterbody.

As indicated previously the detailed fluid mechanics within the separated flow region is not well defined. The problem is complicated still further by the fact that estimates of the flow properties within this region indicate that over the altitude range extending from 150 kft to 350 kft local flow regimes extending from continuum flow to free molecule flow will be experienced. There are indications that over these flow regimes the details of the separated flow patterns change considerably. In order to obtain some idea of the flow within the separated region over the afterbody one must resort primarily to the work done in the studies of flow behind bluff based bodies. Following the work of Refs. 28, 29, and 30 for bluff based bodies it appears that the differences between high and low Reynolds number flows can be qualitatively described as shown in Fig. 32. At high Reynolds numbers the mixing region has a relatively small width dimension and the axial extent of the recirculation region is relatively large. On the other hand for low Reynolds numbers (in the Stokes flow regime) the width of the mixing layer becomes very large and the axial extent of the recirculation region becomes relatively small. The corresponding details of the separated flow over the afterbody of the Apollo can only be conjectured at this time. If one extrapolates the high Reynolds number results obtained for bluff based bodies one might expect a flow pattern similar to that shown in Fig. 33a. At low Reynolds numbers one could expect a greatly reduced width of the recirculation region as shown in Fig. 33b. It is equally possible with the limited knowledge we have at the present time to conjecture that reverse flows over the major portion of the afterbody will not exist except for a small recirculation region near point "B." The velocity profiles from A - B in this case could have the character of incipient separation profiles. In any event, at low Reynolds numbers it appears that the low velocity regions will be close to the afterbody surface and the velocity gradients within the separated region will be smaller than those experienced at higher Reynolds numbers. It is clear in view of the above that in order to determine the location and required travel of the separated flow electron density probe, detailed experimental studies of the separated flow region over an extended range of Reynolds numbers are required.

B. Preliminary Considerations of Probe Location

With the limited information available at the present time we can assume that the high Reynolds number cases under which the probe will operate will determine the maximum distance which the probe will have to extend from the surface of the afterbody. It is assumed that measurements will be made on the leeward side of the vehicle in the pitch plane. In this case, it is estimated, based on the flow geometry discussed previously that if the probe were located about 30 inches from the front heat shield shoulder the probe head will have to be located not more than 18 inches from the afterbody surface. Should detailed design of the probe support indicate a shorter length would be desirable the probe can be moved to a more forward location.

There are several methods of erecting the probe which can be considered. One method would be the simple telescoping of the probe outward from the surface (Fig. 34a). This method may require excessive penetration of the interior of the spacecraft. A means of minimizing the penetration of the spacecraft interior is shown in Fig. 34b. Here in the retracted position the probe-support assembly is in a recess in the surface and is rotated into position as shown. Some penetration of the spacecraft interior is necessary for detection of the final position of the probe. The final selection of the method of probe location will be determined by the overall range of positions which will have to be covered as found by detailed studies of the afterbody separated flow.

For both methods of probe positioning considered it appears that a suitable method of protecting the probe head and support prior to the measurement period is to surround it with an actively cooled heat protective shell as shown in Fig. 35. The protective shell and probe-probe support assembly are moved into position as a unit prior to the time when measurements are made. When measurements are to be made the probe-probe support assembly is held fixed and the shell is partially retracted into the spacecraft. The outside diameter of the shell is estimated to be about 2 inches. This 2 inch dimension roughly corresponds to the relative probe to separated flow field dimensions found in Ref. 30 which resulted in negligible flow field perturbations.

The previous considerations concerning the wide range of flow regimes and flow patterns in the separated flow region indicate that a specific mode of locating the probe head in an area suitable for electron density measurements must be devised taking account of these factors. Let us consider first that the measurements are to be made during the first entry into the sensible atmosphere, in the altitude range extending downward from 350 kft to 200 kft where the spacecraft begins to ascend again to an altitude of about 300 kft. As indicated, there is considerable uncertainty about the nature of the recirculating flow at the higher altitudes, while at 200 kft one might expect a conventional recirculation region imbedded in the separated flow. It is suggested (pending detailed experimental studies of separated flow over a wide range of Reynolds numbers) that the following mode of operation be considered. Prior to passing through the 350 kft altitude the probe head is set at a relatively small distance from the surface of the afterbody (three to six inches). This location is chosen because best estimates in this altitude range indicate that the Mach number will remain below 0.3 regardless of the detailed flow pattern. For such low values of Mach and

Reynolds numbers no substantial perturbations of the electron density distribution are anticipated. Measurements of electron density would be taken until pressure sensors employing orifices located at the front and back of the probe heat shield indicate a detectable pressure difference. With the sensitivity of "off the shelf" strain gage pressure transducers the first indication of a sensible pressure difference is expected to occur at an altitude near 250 kft. If the pressure difference indicates a recirculating flow the probe is moved outward to a location where the pressure difference is again equal to the minimum detectable value.

C. Inflight Measurement System

The arrangement presented below provides for the positioning of the probe, the measurement of electron density, and the recording of data during a reentry application. The sophistication of the system reflects the lack of available information describing the aerodynamic conditions in the region of interest. An inflight application, however, should be preceeded by a theoretical and experimental investigation of the separated flow region. The results of such a study may allow for a considerable simplification of the system, especially with respect to the probe positioning mechanism.

The proposed system is shown in Fig. 36. The main components are a programming circuit which gives the sequence of operations, furnishes a warm-up period for the electronic equipment, and commands the erection and retraction of the probe. Also included are a microwave generator which feeds the probe with a signal which is frequency modulated and monitored, a ramp generator to modulate the microwave generator, a calibration unit which furnishes a permanent check of the correspondence between modulating signal and frequency, a multiplexing circuit to collect the probe and calibration unit outputs, and a recording system to store these outputs. Besides these, there is the erecting device which swings the probe from its housing to the measuring position, a differential pressure sensor which detects the region of very low velocity, a positioning servo to move the probe and its heat shield until the pressure sensors find an adequate position for the measurement, and a heat shield removal control. The probe positioning system is shown schematically in Fig. 37. It is seen that the probe is located coaxially with the positioning arm, this configuration has been chosen in order to simplify the removal of the heat shield. To position the probe near the region of zero flow a pressure sensing device is used. The probe is initially surrounded by a heat shield which contains two orifices located in the plane of gas flow. These orifices then pick up the pressure up- and downstream of the probe and transmit it to a differential pressure gage located inside the vehicle. The resolution of a typical gage is on the order of 50 microns Hg pressure. A correspondence between differential pressure and gas velocity is difficult to estimate. However, an arrangement similar to that described here has been used to determine the zero flow line in the near wake of a cone at Mach 6 with pressures on the same order of magnitude as those encountered in this application (Ref. 30). To a first approximation the pressure in the downstream orifice can be taken as static while the upstream can be taken as the total pressure. To reach a differential pressure equal to the resolution of the gage the Mach number of the flow around the probe, for an altitude of 200 kft (approximately $t = 1.5$ minutes in Fig. 1) for instance, should have a minimum value of 0.1.

The heat shield is designed to protect the probe during the erecting and positioning period. This shield has a double wall with a cooling fluid flowing through them in order to extend its duration in this environment. Figures 36a and 36b show the top and side views, respectively, of the mechanical system in the retracted position. To perform the measurement the arm is rotated 90° around an axis parallel to the surface of the vehicle. At this moment the positioning actuator (commanded by the differential pressure detector) slides the probe and shield until the pressure difference is below the resolution of the gage. The probe is then locked in position and the heat shield actuator slides back the shield, exposing the probe. After the measurement has been performed the program commands the shield to cover the probe and retracts the arm.

The electronic circuit which provides a calibrated frequency modulated microwave signal and gives the output of the probe in a suitable form is shown in Fig. 38. It includes a microwave generator which can cover the range of operating frequencies required by the probe. A solid state oscillator is suitable for this application. A ramp generator modulates the frequency of the microwave signal.

The shape of the signal at various points along the circuit is shown in Fig. 39. For each sweep of the ramp generator a resonant peak is detected. This signal is then amplified and cut as shown. The resulting square pulse is used as a gate to allow a portion of the ramp signal to reach a voltage holding circuit. The voltage level at this point is then directly related to the resonant frequency of the probe.

An additional circuit is included which furnishes three calibration points to check the correspondence between voltage level (last signal from probe in Fig. 39) and microwave frequency at the voltage holder. The same signal fed to the probe is fed to three microwave resonant cavities working in the transmission mode with known resonant frequencies in the range of operation of the probe. The output of each reference cavity goes through a circuit entirely similar to the one just described for the probe. The four D.C. voltage levels, one from the probe and one from each reference cavity are then multiplexed, encoded and recorded.

The sequence of operation of the total system must be chosen to be compatible with the exposure time of the probe. A heat transfer computation indicates that the probe element may last for several minutes, however other factors may be much more restrictive. The expansion and variation of dielectric constant of the boron nitride tube due to heating impose severe restrictions on the measuring time. A study of both effects indicates that the dielectric variation predominates, and that the combined effect at a typical reentry condition produces a shift in resonant frequency equal to the resolution of the probe in a time on the order of two seconds. This effect is particularly important at lower electron densities. In order to overcome this restriction a technique may be employed where the probe is exposed for a period of two seconds, retracted into a cooling condition, and then re-emersed in the plasma in a repetitive manner.

The system described is merely a preliminary design and must of course be redesigned to be compatible with a specific spacecraft and trajectory. For the design presented a preliminary estimate of weight and volume has been made. In principle it can be accepted that the programming circuit and recording equipment are already included in the vehicle and that their bulk will not be appreciably increased because of this measurement. The equipment can be arranged in two physical groups, the probe housing and the electronic package. The former contains the probe, heat shield, heat shield and positioning actuators, the erecting mechanism, and the differential pressure gage. The latter contains the microwave and ramp generators, the calibration unit, the audio amplifiers and shapers, a multiplexor and encoder, and a differential pressure amplifier. It has been estimated that the probe housing will weight approximately eight pounds and have a volume of four hundred cubic inches, while the electronic package will weight approximately nine pounds and have a volume of twenty-five hundred cubic inches.

XI. Conclusions and Recommendations

Conclusions

1. A probe capable of measuring electron densities in the range 10^{10} to 10^{14} e/cm^3 has been developed for use in a superorbital shock tube tunnel in conditions simulating the separated flow region of a reentering Apollo vehicle.

2. Three possible schemes of operation have been considered, their characteristics were evaluated and the one most suitable for an inflight application, namely resonant frequency shift, was selected.

3. The Q of the electromagnetic resonant structure is found to be greater than 1000 throughout the entire range of operating frequencies, thus providing the required sensitivity.

4. The size of the probe and its coupling have been reduced to a minimum value for the selected range of operating frequencies. Both input and output couplings are provided on the same side of the probe, and a unique correlation is attained between resonant frequency and electron density through proper mode discrimination.

5. The effects of charge diffusion and heat transfer will not appreciably affect the operation of the probe for the particular flight trajectory taken in this study.

6. A calibration of the probe was performed in the lowest range of electron densities with a plasma simulating plastic foam, in the middle range with shock tube and electrical discharge produced plasmas and in the upper range by using metallic cylinders to simulate highly overdense plasmas.

7. An inflight application of the probe is possible utilizing standard microwave equipment.

8. A considerable reduction in the complexity of the proposed system for an inflight application may be realized with a better knowledge of the conditions existing in the separated flow region.

Recommendations

1. The dimensions of the probe should be reduced in order to minimize the perturbation of the surrounding medium. It is recommended that this reduction be attained by decreasing the operating wavelength by a factor of three with a corresponding scaling of the probe dimensions (Ref. 33).

2. An analytic and experimental study should be made of the separated flow field of a reentering Apollo vehicle for various flight conditions in order to determine the effects of the local environment upon the operation of the probe and in turn the effect of the probe on the environment.

Particular emphasis should be placed on the effects of heat transfer, charge diffusion, and a finite velocity about the probe, upon the electron density measurement.

3. The effect of the ablation products coming from the main heat shield of the Apollo vehicle on the electron density levels in the region where the probe is supposed to operate should be determined.

REFERENCES

1. Development of a Probe to Measure the Electron Density in Separated Flow Regions Surrounding the Apollo Vehicle, GASL Proposal No. 9-440 (Technical), September 15, 1964.

2. Abele, M., Theory of Propagation of an Electromagnetic Field in a Dielectric Circular Waveguide, Nuovo Cim., Vol. 5, N. 4, August 1948.

3. Robson, P. N. and Stewart, R. D., Surface Wave Probe for Measuring Electron Densities in a Gaseous Plasma, Electronic Letters, Vol. 1, No. 1, March 1965.

4. Abele, M., Byrne, R. W., and Medecki, H., Development of a Probe for the Measurement of Point Values of Electron Densities in Supersonic Flows, GASL TR-527, April 1965.

5. Harvey, A. F., Periodic and Guiding Structures at Microwave Frequencies, IRE Trans. on Microwave Theory and Techniques, January 1960.

6. Barlow, H. M. and Brown, J., Radio Surface Waves, Oxford University Press, London, 1962.

7. Collin, R. E., Field Theory of Guided Waves, McGraw-Hill Book Co., New York, 1960.

8. Hutter, R., Beam and Wave Electronics in Microwave Tubes, D. VanNostrand Co., New York, 1960.

9. Rotman, W., A Study of Single-Surface Corrugated Guides, Proc. IRE, August 1951.

10. Rosenbaum, F. J., Dielectric Cavity Resonator for ESR Experiments, Rev. of Scient. Instr., Vol. 35, No. 11, November 1964.

11. Duncan, J. W. and DuHamel, R. H., A Technique for Controlling the Radiation from Dielectric Rod Waveguides, IRE Trans. on Antennas and Propagation, July 1957.

REFERENCES

12. Becker, R. C. and Coleman, P. D., The Dielectric Tube Resonator, Proceedings of the Symposium on Millimeter Waves, Polytechnic Press of the Polytechnic Institute of Brooklyn, New York, Vol. 9, pp. 191-222, 1959.

13. Iiguchi, Shin-ichi, Mode Conversion in the Excitation of TE_{01} Waves in a TE_{01} Mode Transducer, Proceedings of the Symposium on Millimeter Waves, Polytechnic Press of the Polytechnic Institute of Brooklyn, New York, Vol. 9, pp. 595-618, 1959.

14. Wolfert, P. H., A Wide-Band Rectangular-to-Circular Mode Transducer for Millimeter Waves, IEEE Trans. on Microwave Theory and Techniques, September 1963.

15. Abele, M. and Medecki, H. Development of a Probe for the Measurement of Point Values of Electron Densities in Supersonic Flows, presented at the Third Symposium on the Plasma Sheath, Bedford, Mass., September 1965.

16. Lin, S., Resler, E., and Kantrowitz, A., Electrical Conductivity of Highly Ionized Argon Produced by Shock Waves, J. Appl. Phys., Vol. 26, No. 1, January 1955.

17. Petschek, H. and Byron, S., Approach to Equilibrium Ionization Behind Strong Shock Waves in Argon, Annals. Phys., Vol. 1, pp. 270-315, 1957.

18. Resler, E., Lin, S., and Kantrowitz, A., The Production of High Temperature Gases in Shock Tubes, J. Appl. Phys., Vol. 23, No. 12, December 1952.

19. Morgan, E. and Morrison, R., Ionization Rates Behind Shock Waves in Argon, Phys. Fluids, Vol. 8, No. 9, September 1965.

20. Duff, R., Shock Tube Performance at Low Initial Pressure, Phys. Fluids, Vol. 2, No. 2, March 1959.

21. Lamb, L. and Lin, S., Electrical Conductivity of Thermally Ionized Air Produced in a Shock Tube, J. Appl. Phys., Vol. 28, No. 7, July 1957.

22. Lin, S., Neal, R., and Fyfe, W., Rate of Ionization Behind Shock Waves in Air, I. Experimental Results, Phys. Fluids, Vol. 5, No. 12, December 1962.

23. Sturtevant, B., Diffusion in a Slightly Ionized Gas with Application to Effusion from a Shock Tube, Phys. Fluids, Vol. 4, No. 9, September 1961.

24. Bird, G. A., Aerodynamic Properties of Some Simple Bodies in the Hypersonic Transition Regime AIAA Journal, Vol. 4, No. 1, January 1966, pp. 55-60.

25. Baldwin, L. V., Sandburn, V. A., and Laurence, J. C., Heat Transfer from Transverse and Yawed Cylinders in Continuum, Slip and Free Molecule Air Flows, ASME, Journal of Heat Transfer, May 1960, pp. 77-86.

26. Hansen, C. F., Approximations for the Thermodynamic and Transport Properties of High-Temperature Air, NACA TN 4150, March 1958.

27. Jones, Robert A., Hunt, James L., Recent Experimental Studies on Heat Transfer to the Apollo Command Module - NASA SP-101 - Conference on Langley Research Related to Apollo Mission, Langley Research Center, June 22-24, 1965.

28. Viviand, H. and Berger, S. A., The Base-Flow and Near-Wake Problem at Very Low Reynolds Numbers, J. Fluid Mechanics, Vol. 23, Part 3, 1965, pp. 417-458.

29. Kavanau, L. L., Base Pressure Studies in Rarefied Supersonic Flows, J. Aero. Sci., Vol. 23, No. 3, 1956, pp. 193-207.

30. Martellucci, A., Trucco, H., and Agnone, A., Measurements of the Turbulent Near Wake of a Cone at Mach 6, AIAA Journal, Vol. 4, No. 3, March 1966, pp. 385-391.

31. Proposed Extension of Contract NAS5-9881, Development of a Probe to Measure the Electron Density in Separated Flow Regions Surrounding the Appolo Vehicle, GASL Proposal No. 2-726 (Technical), February 7, 1966.

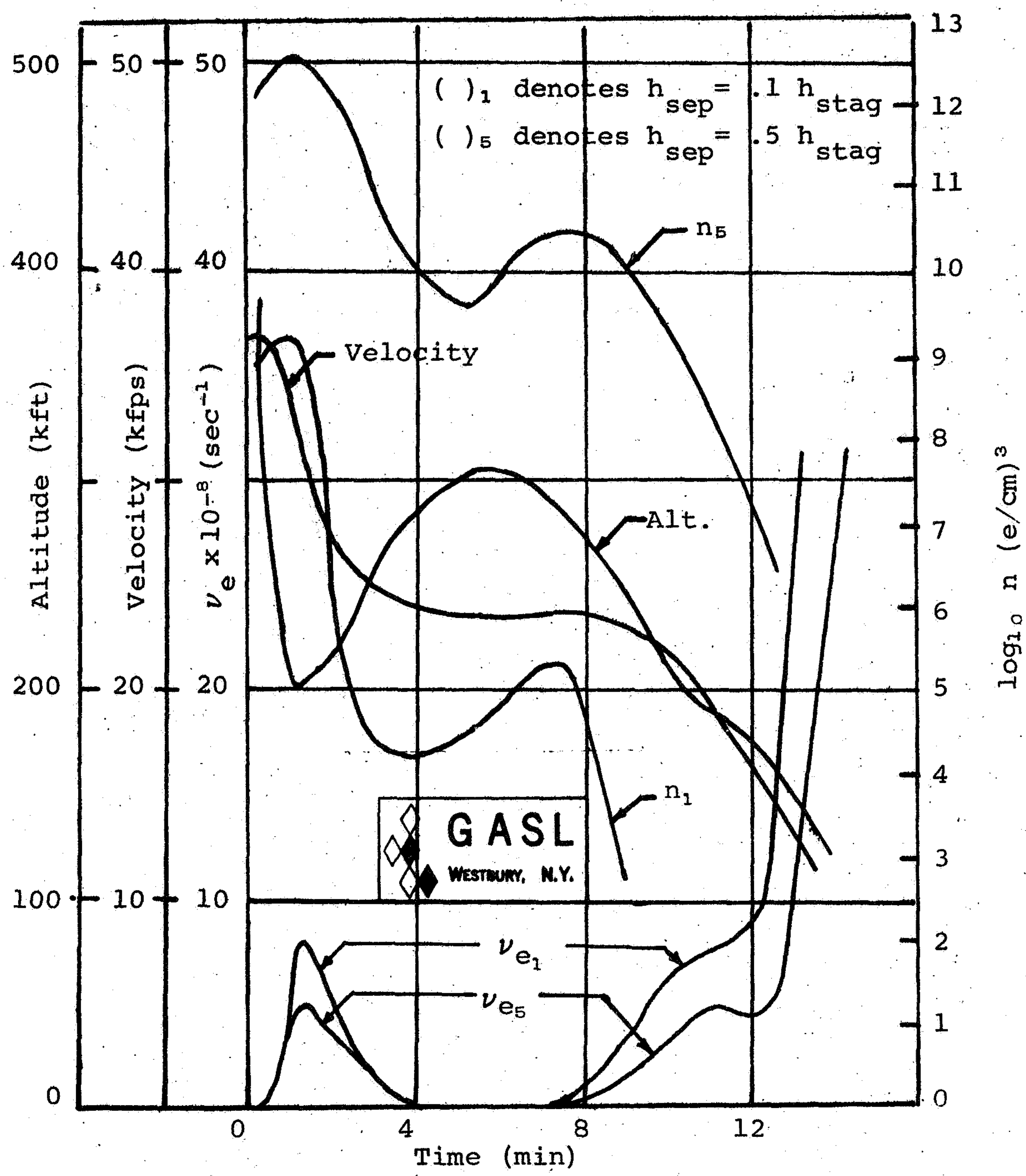

FIG. 1. REENTRY PLASMA PROPERTIES AS A FUNCTION OF ALTITUDE

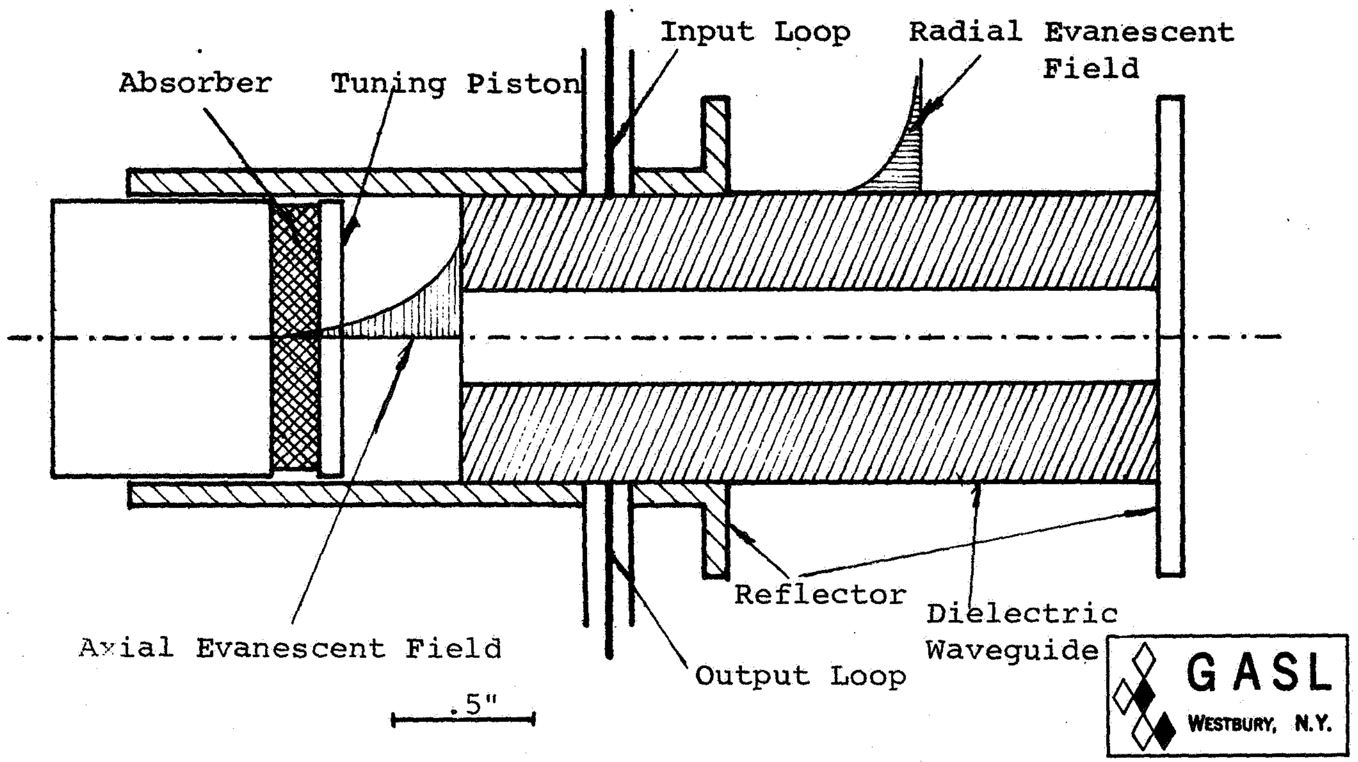

FIG. 2. SINGLE FREQUENCY ELECTRON DENSITY PROBE

NASA Contract NAS5-9881

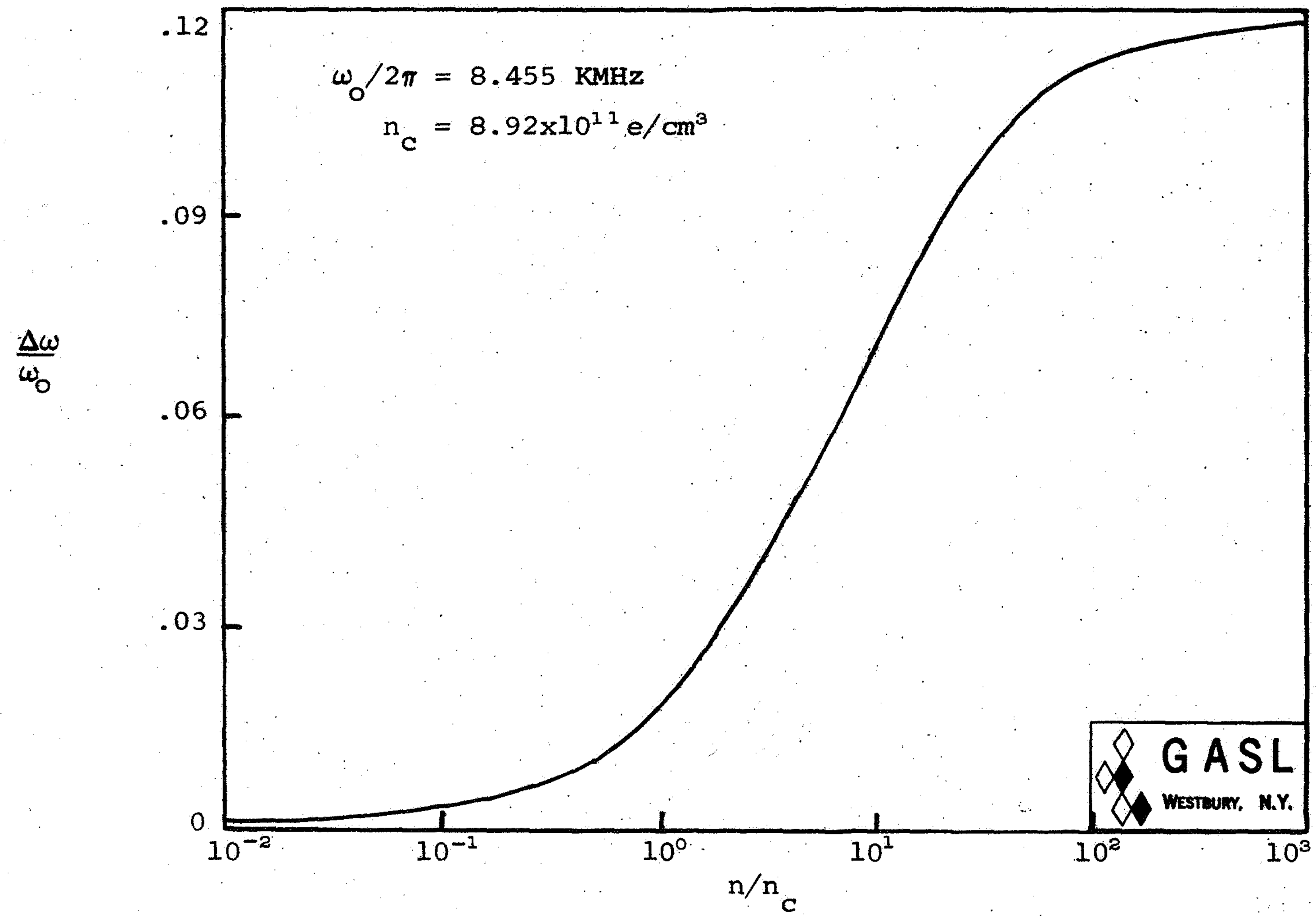

FIG. 3. CHARACTERISTICS OF THE DIELECTRIC PROBE
NASA CONTRACT NAS5-9881

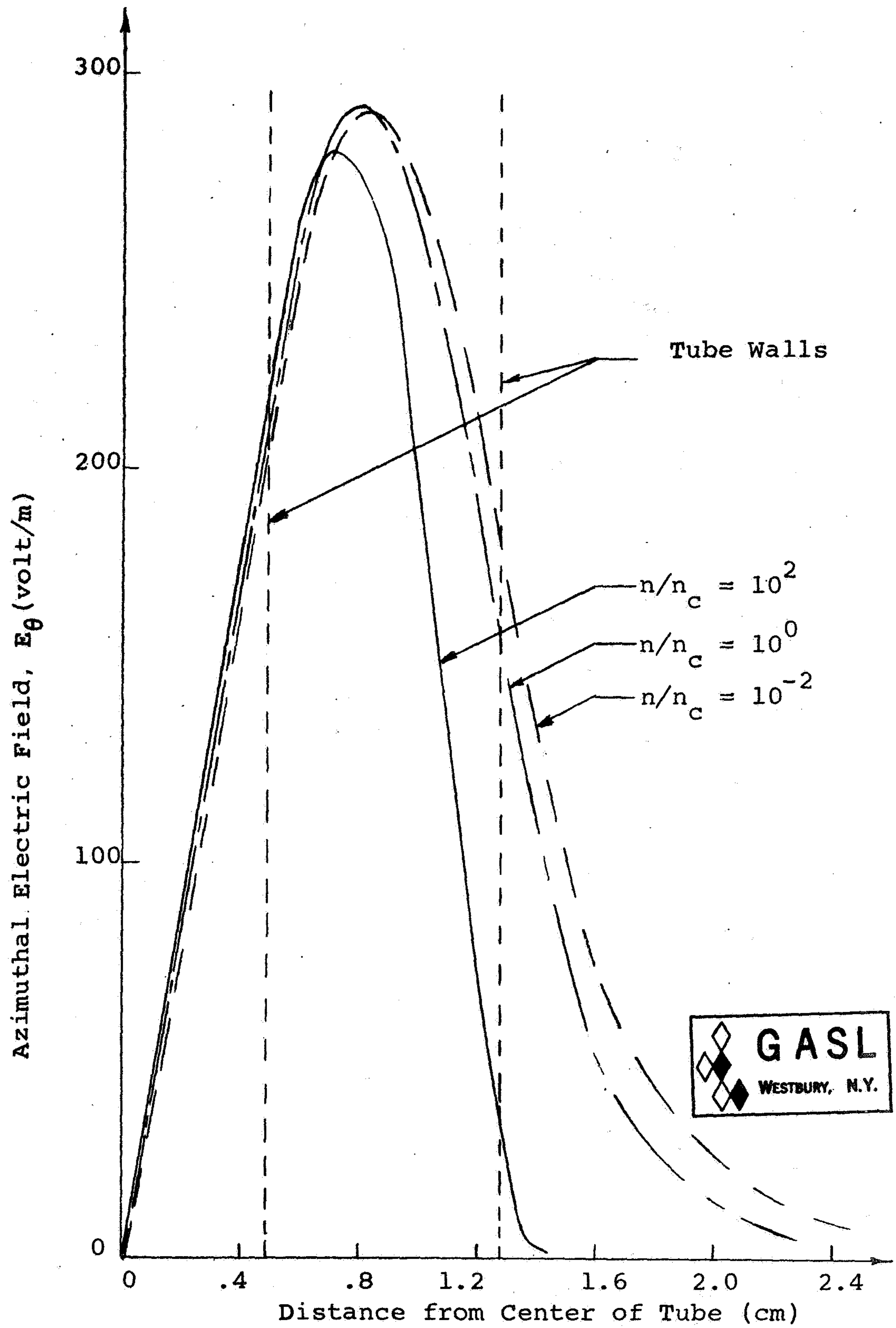

FIGURE 4. ELECTRIC FIELD DISTRIBUTION FOR A DIELECTRIC PROBE

NASA Contract NAS5-9881

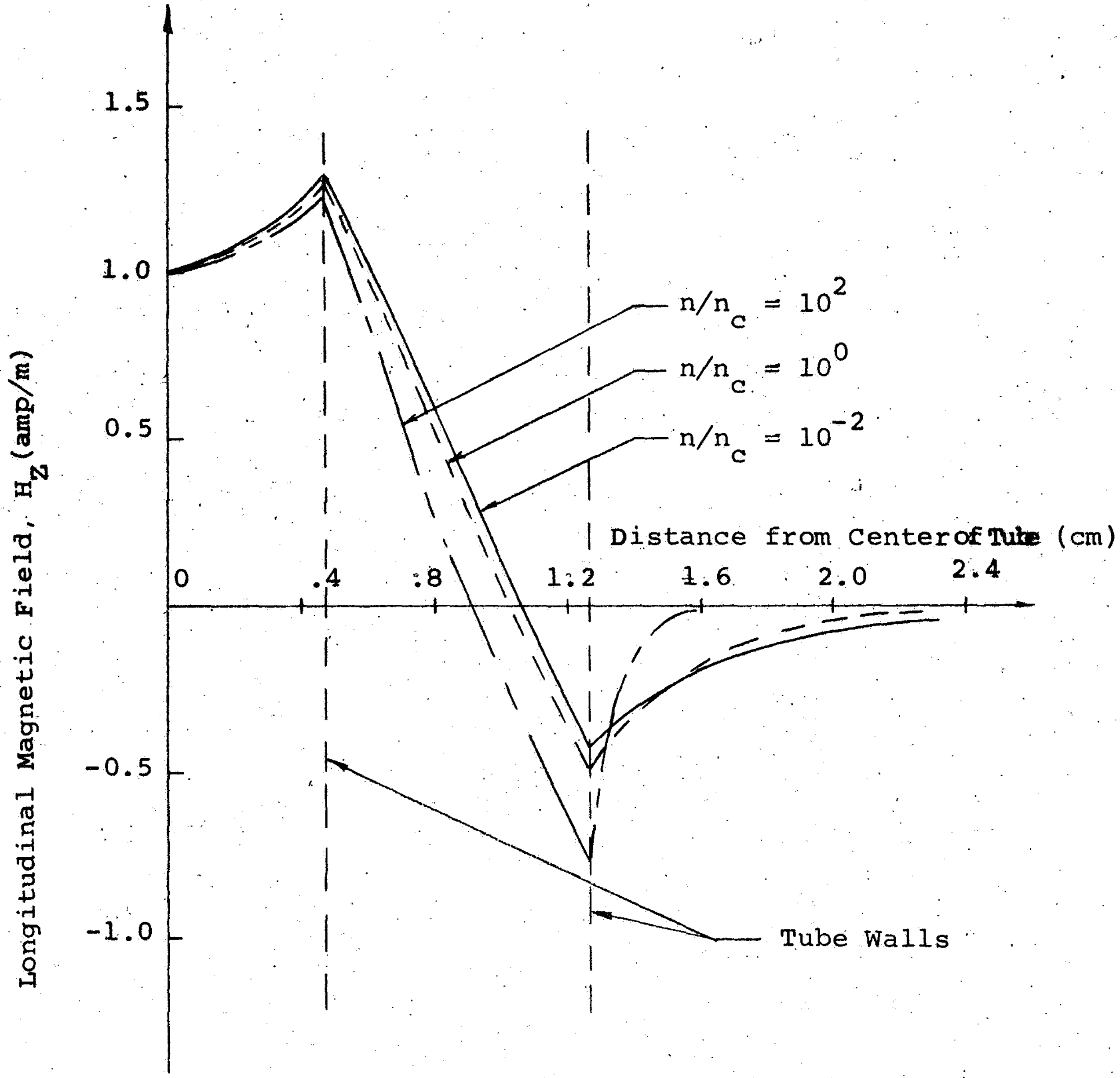

GASL WESTBURY, N.Y.

FIGURE 5. MAGNETIC FIELD DISTRIBUTION FOR A DIELECTRIC PROBE

NASA Contract NAS5-9881

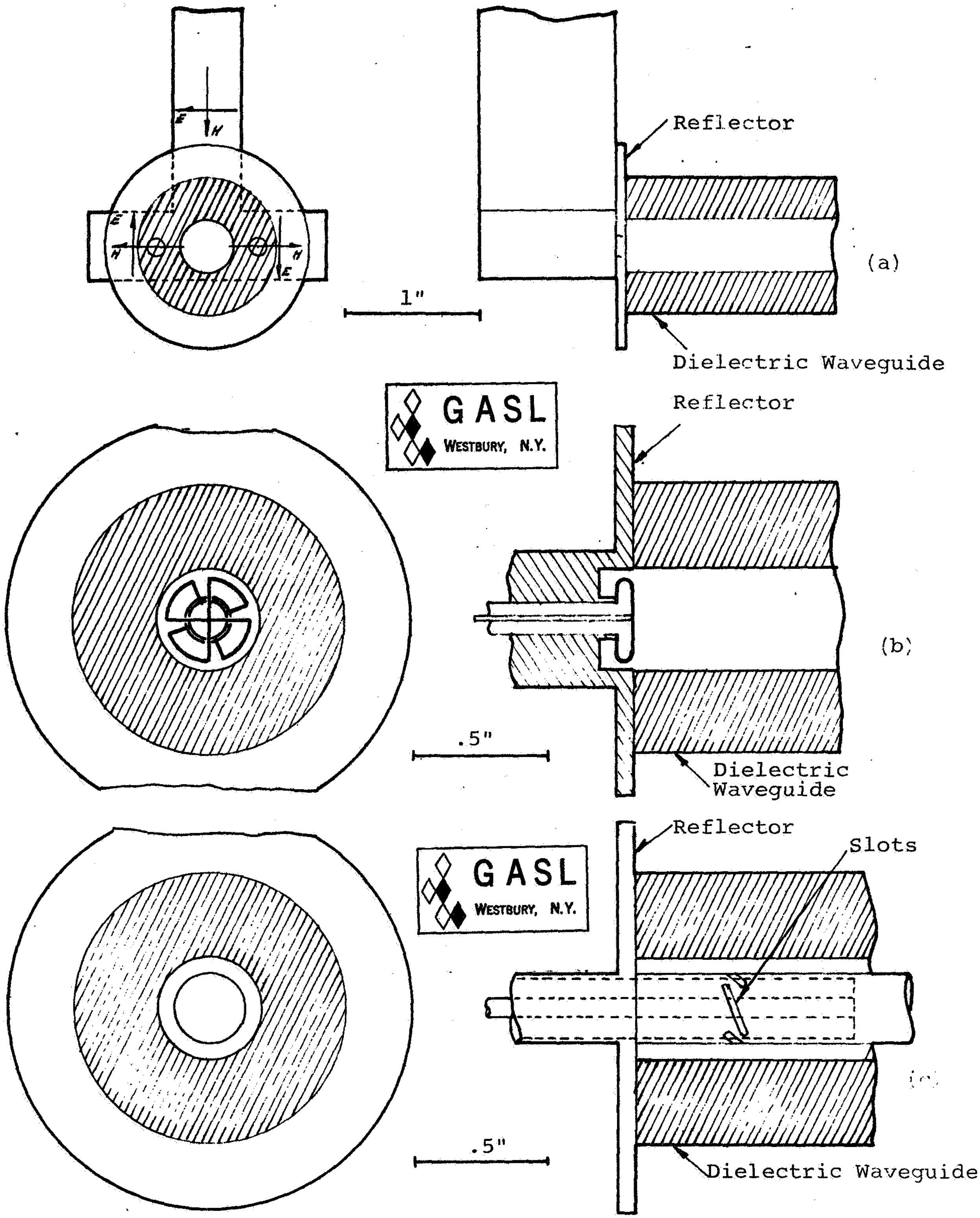

FIG. 6. VARIOUS ELECTROMAGNETIC COUPLING ARRANGEMENTS

NASA Contract NAS5-9881

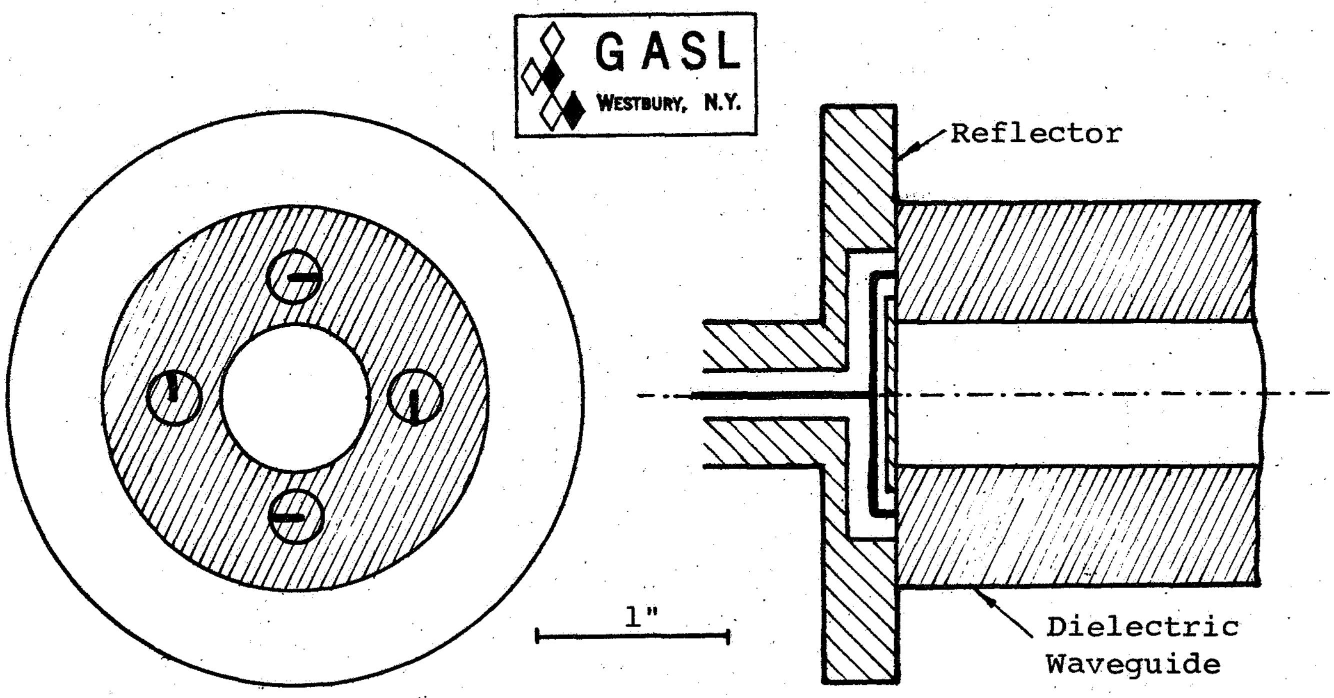

FIG. 7. FOUR LOOP COUPLING

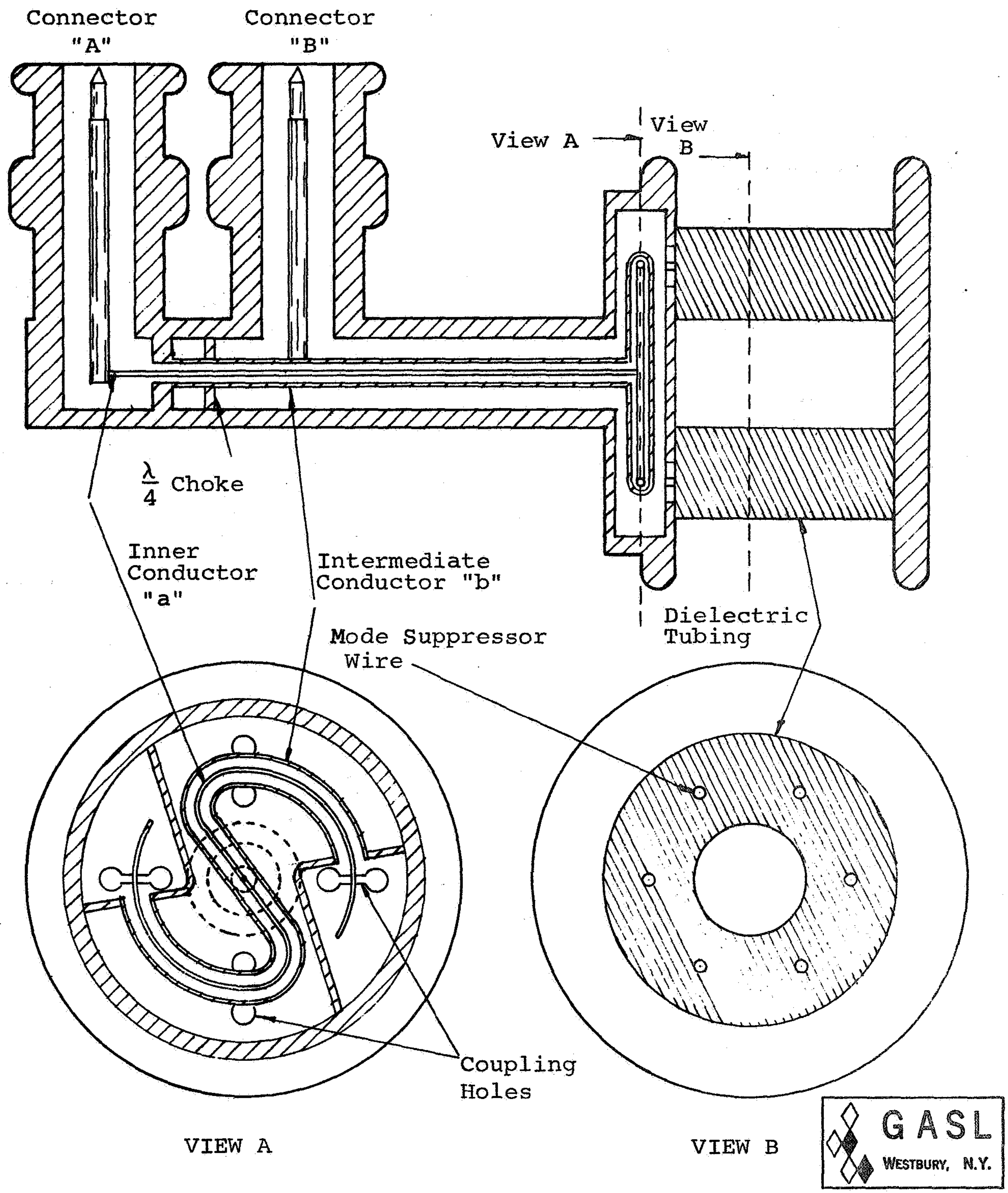

FIG. 8. INTERNAL VIEW OF THE FINAL PROBE

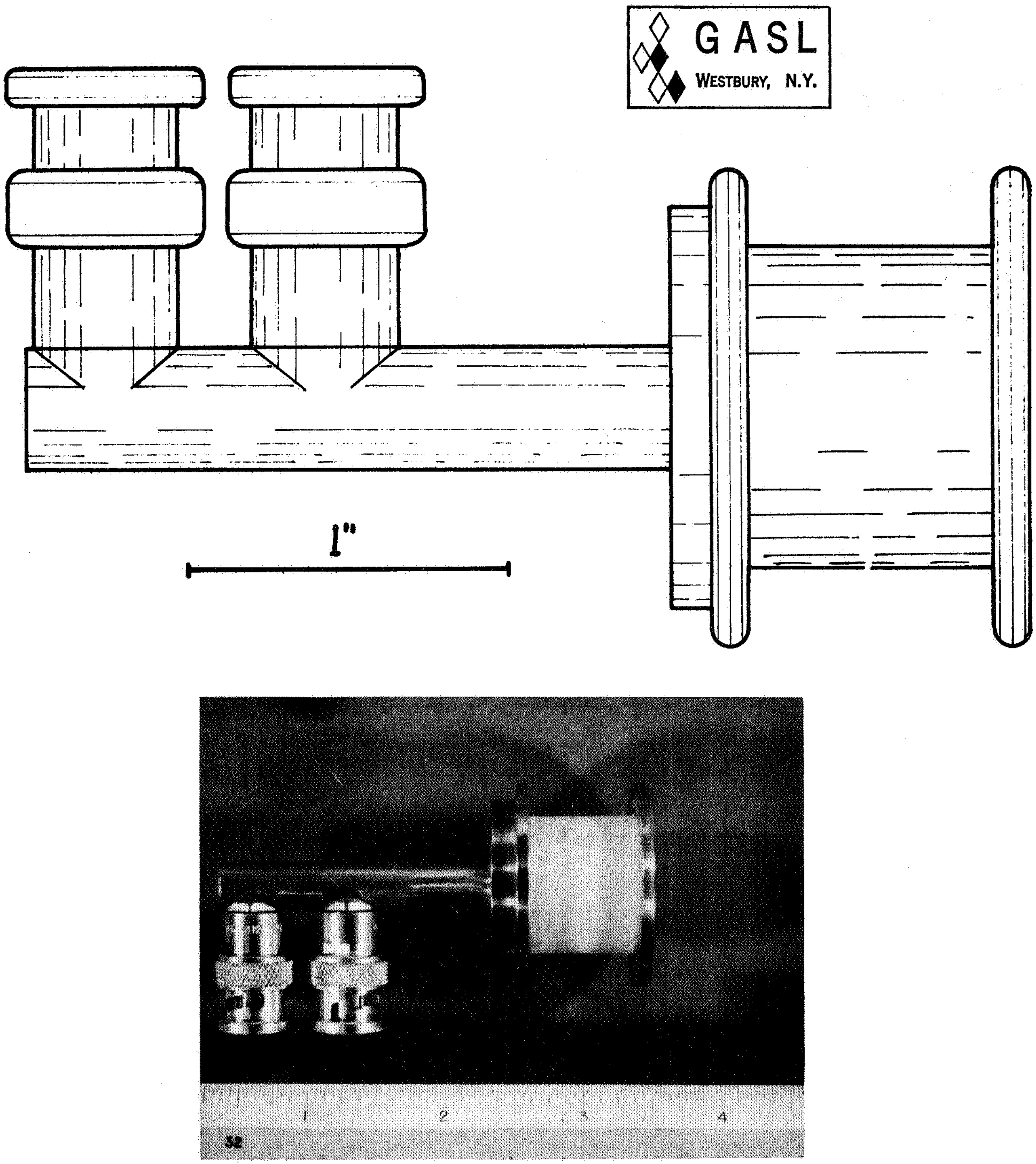

FIG. 9. EXTERNAL VIEW OF THE PROBE

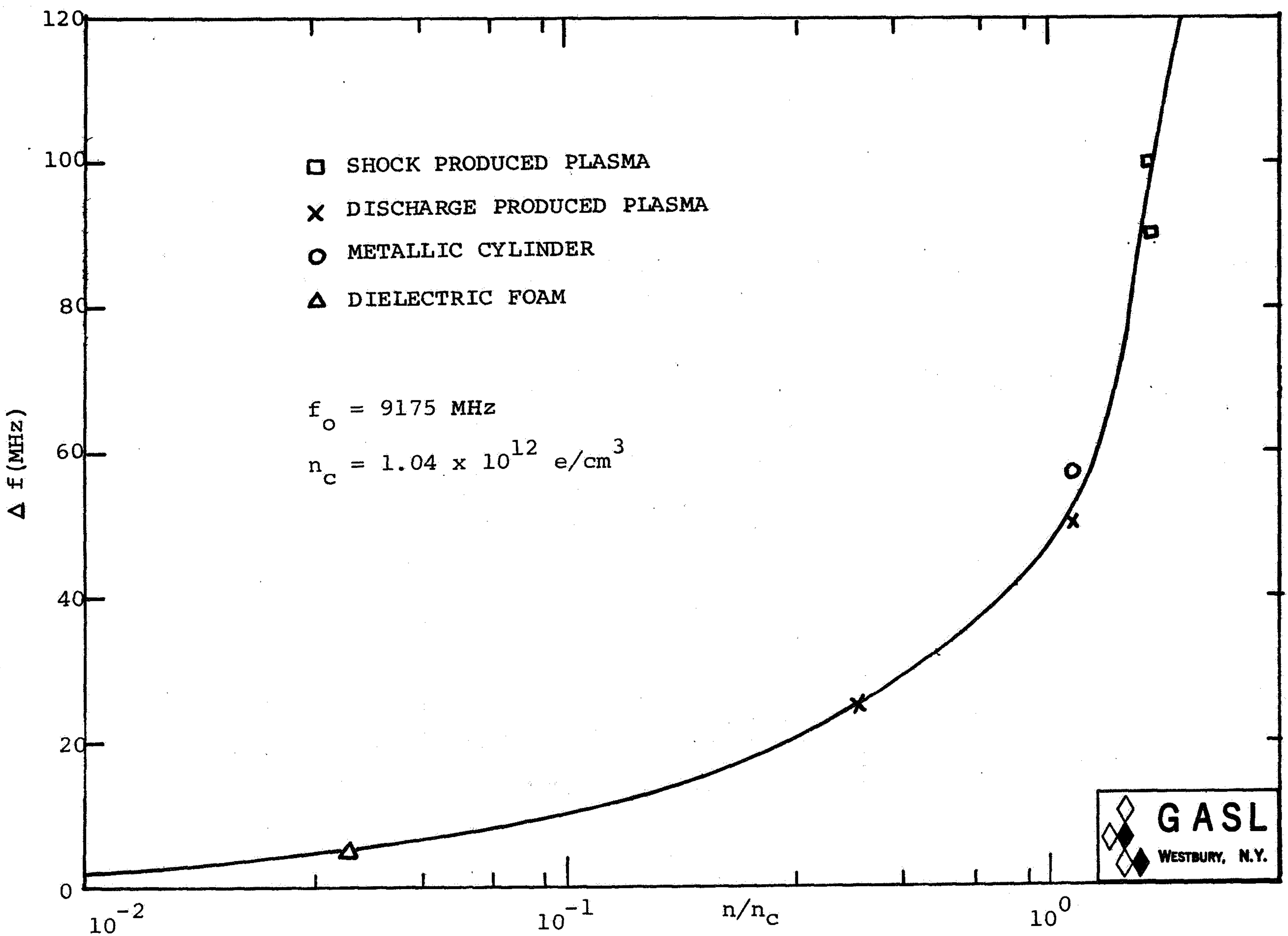

FIG. 10. FINAL CALIBRATION FOR SMALL ELECTRON DENSITIES

NAS5-9881

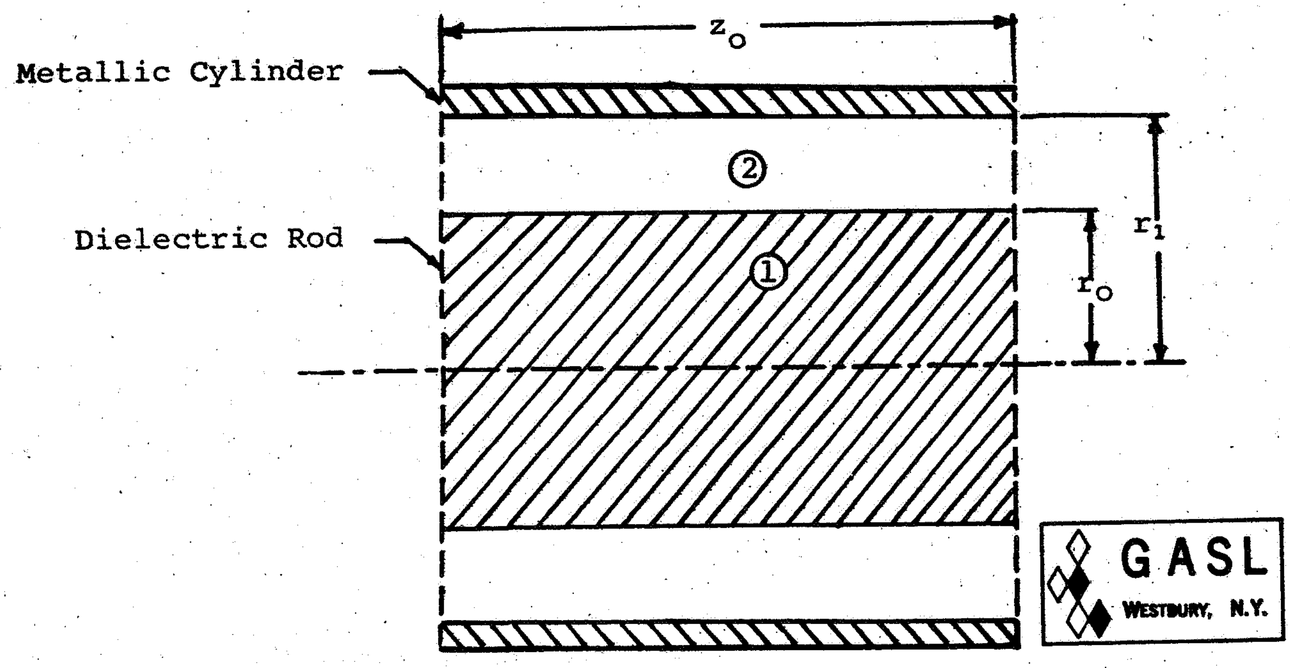

FIG. 11. SECTIONAL DRAWING OF PROBE WRAPPED WITH A METALLIC CYLINDER

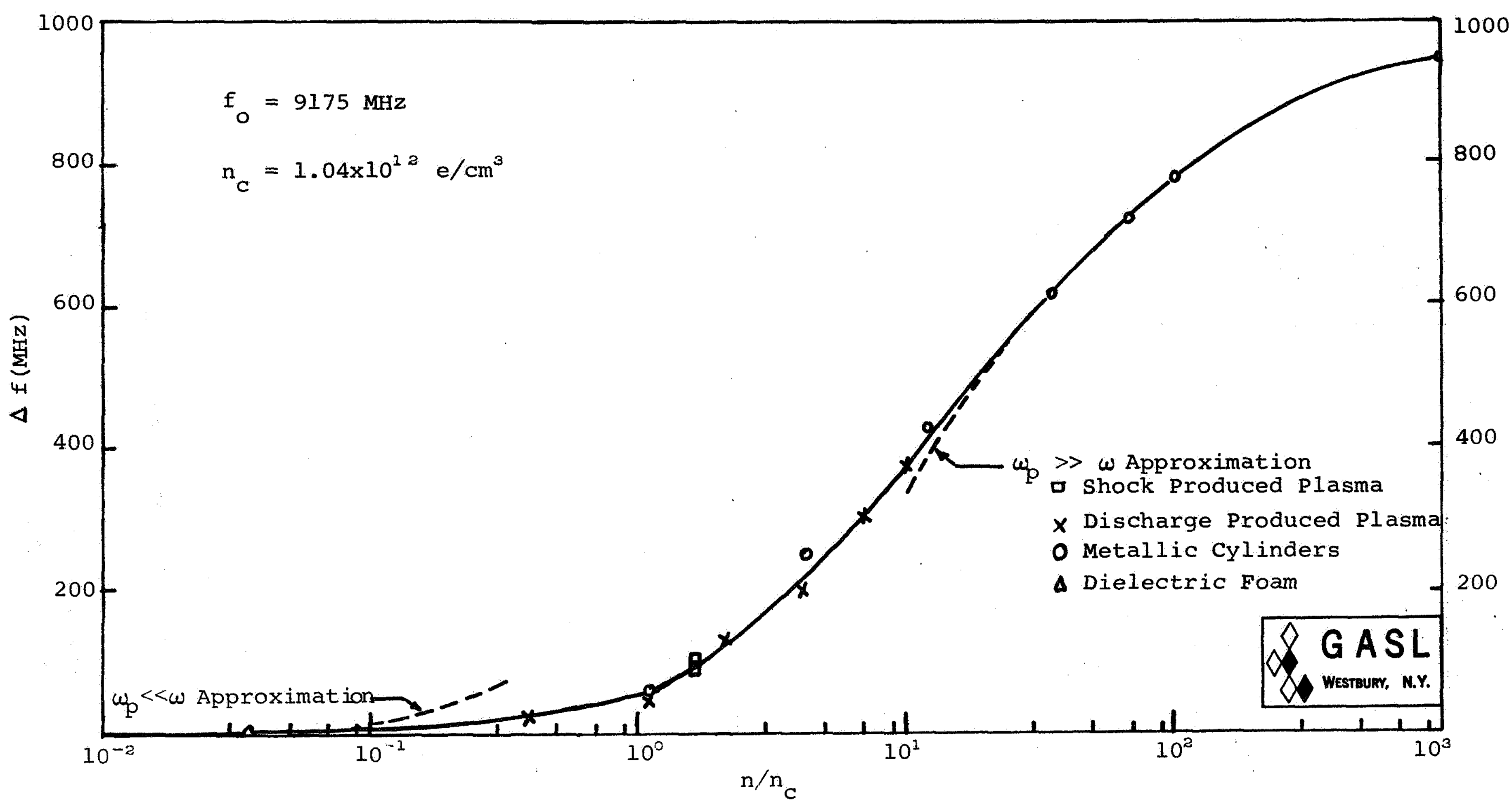

FIG. 12. FINAL CALIBRATION CURVE

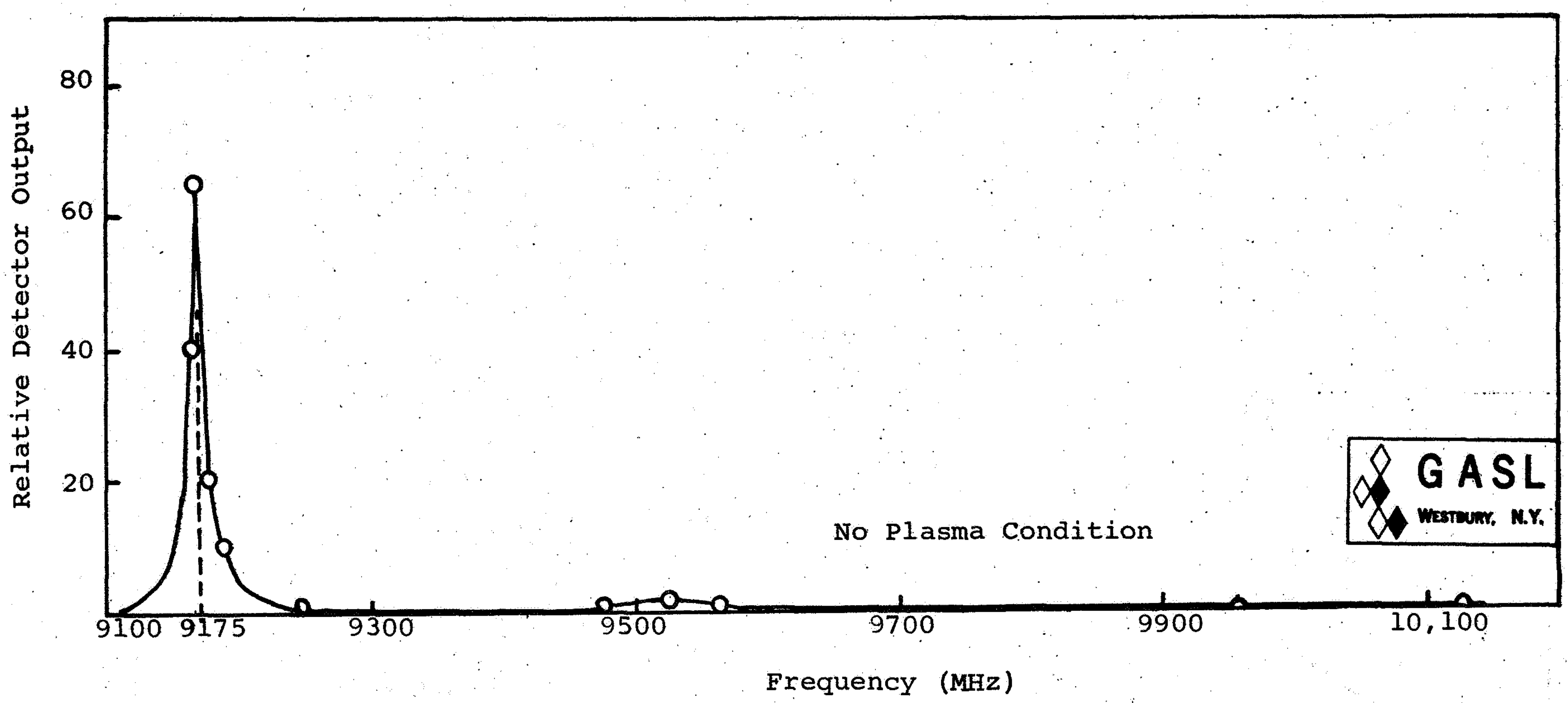

FIG. 13. PROBE OUTPUT THROUGHOUT FREQUENCY RANGE FOR THE NO PLASMA CONDITION

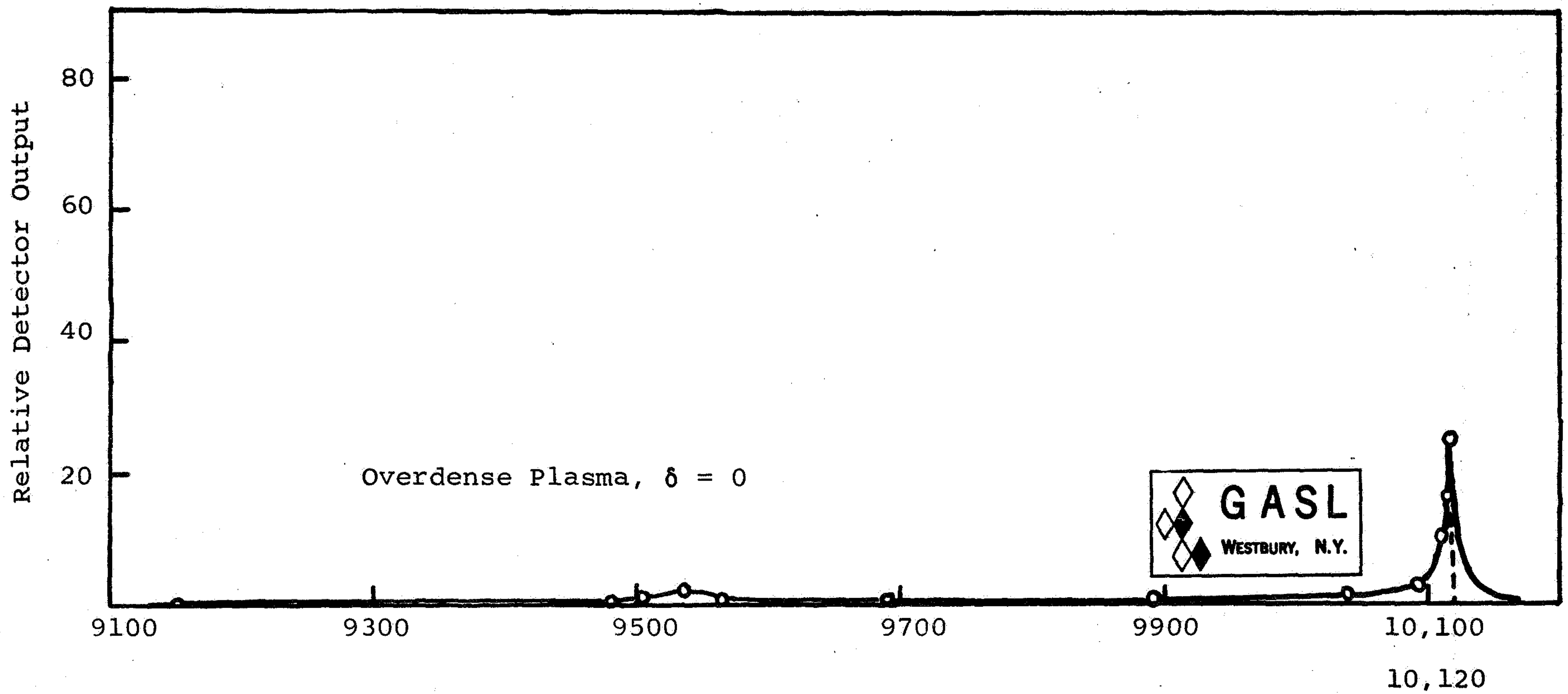

FIG. 14. PROBE OUTPUT THROUGHOUT FREQUENCY RANGE FOR THE HIGHLY OVERDENSE PLASMA CONDITION

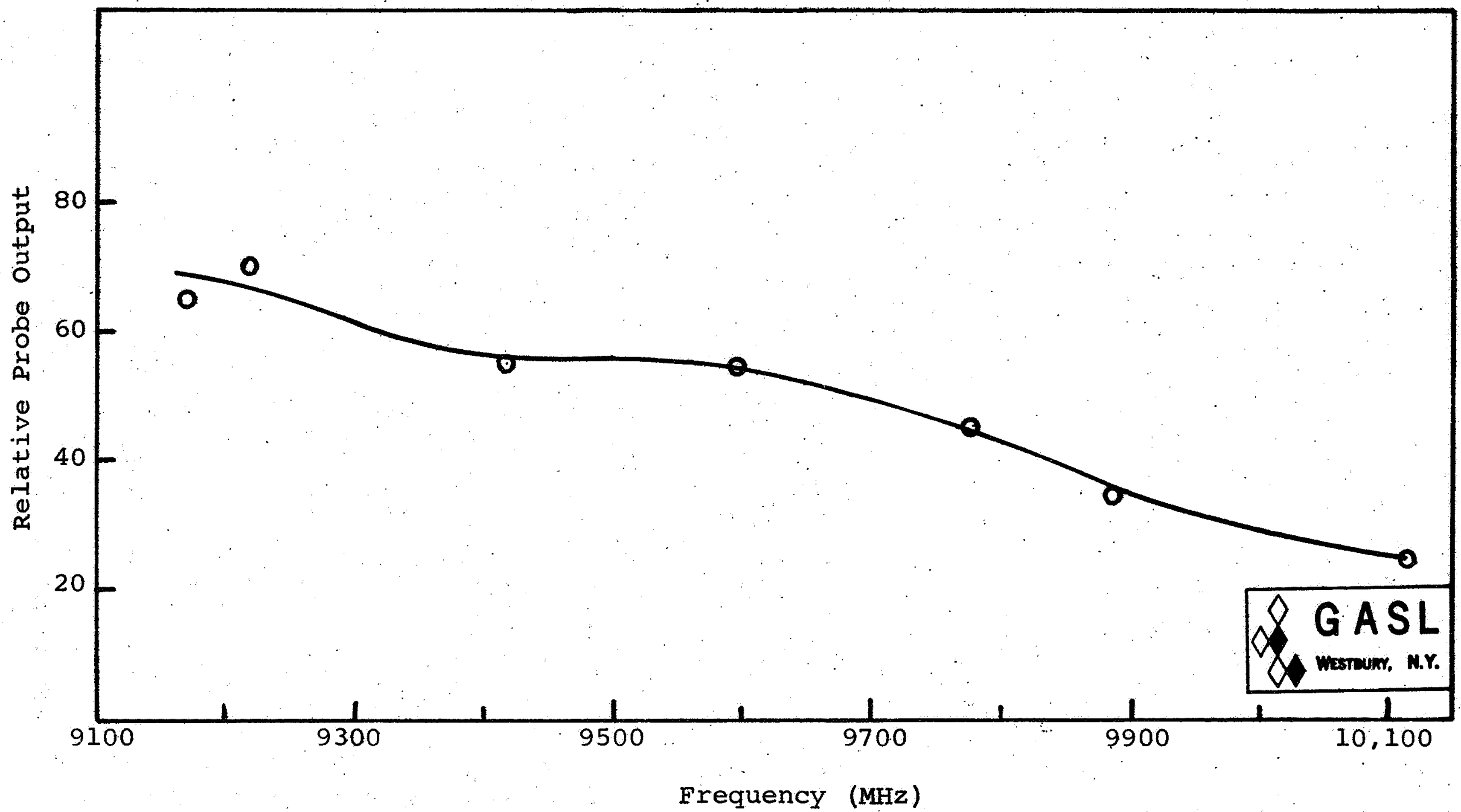

FIG. 15. RESONANCE RESPONSE OF PROBE THROUGHOUT FREQUENCY RANGE

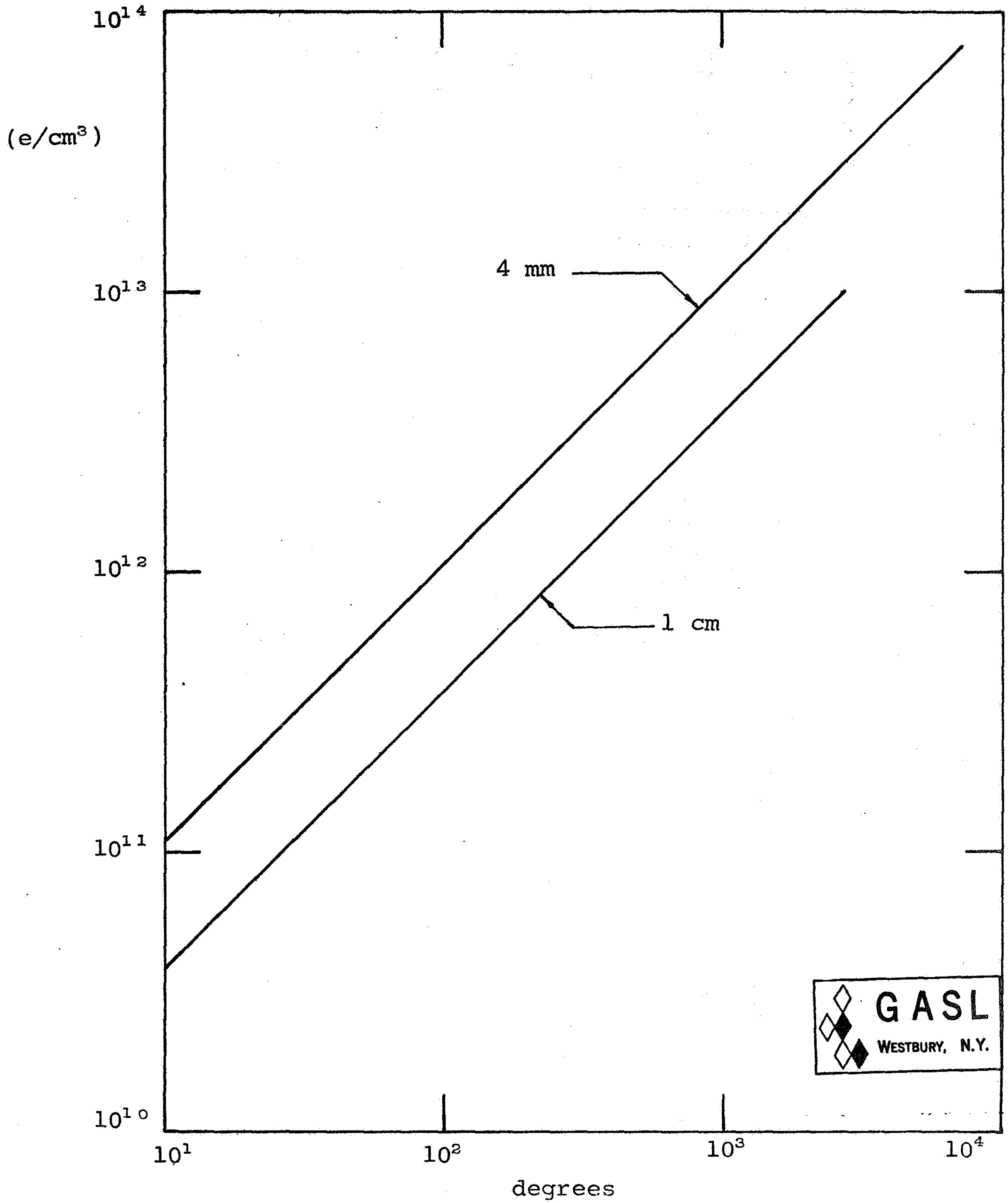

FIG. 16. INTERFEROMETER CALIBRATION CHARTS
NASA Contract NAS5-9881

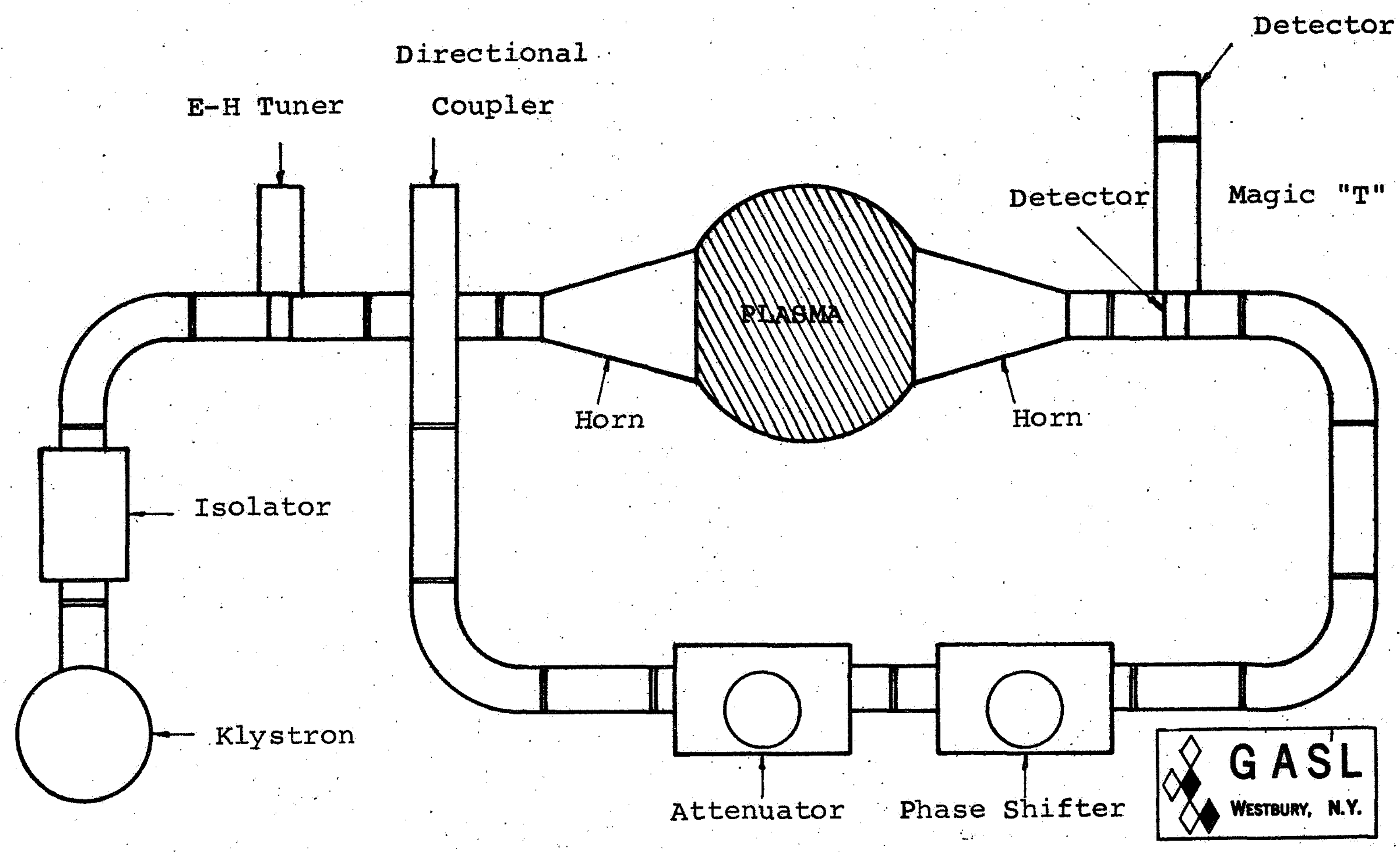

FIGURE 17. SCHEMATIC DIAGRAM OF MICROWAVE INTERFEROMETER

NASA Contract NAS5-9881

a) P_i=.2 mm(Hg) Argon

Time scale = 20 μs/cm

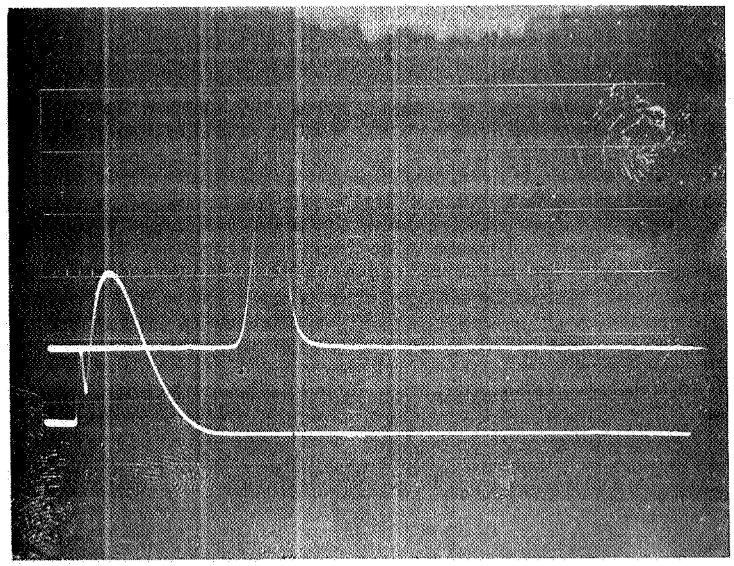

b) P_i=.35 mm(Hg) Argon

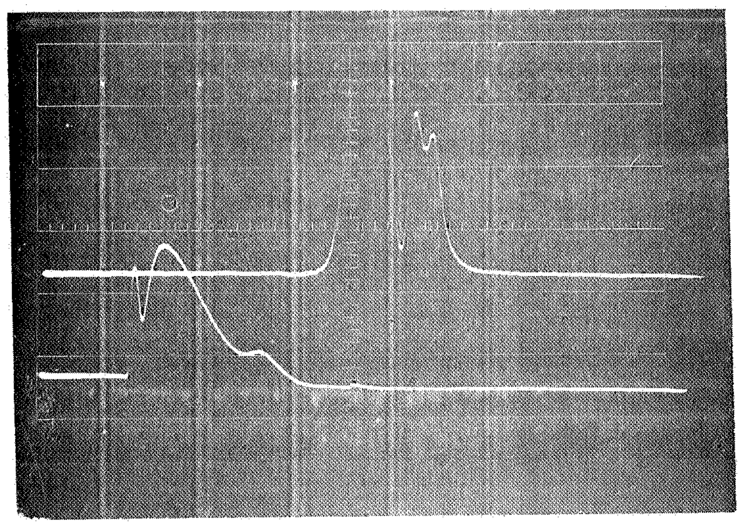

c) P_i=.50 mm(Hg) Argon

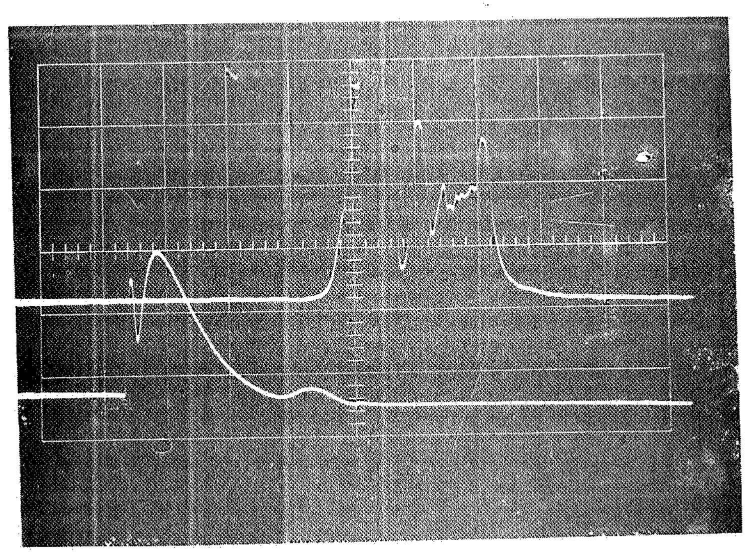

FIGURE 18. ONE cm INTERFEROMETER TRACE OF INCIDENT ARGON PLASMA

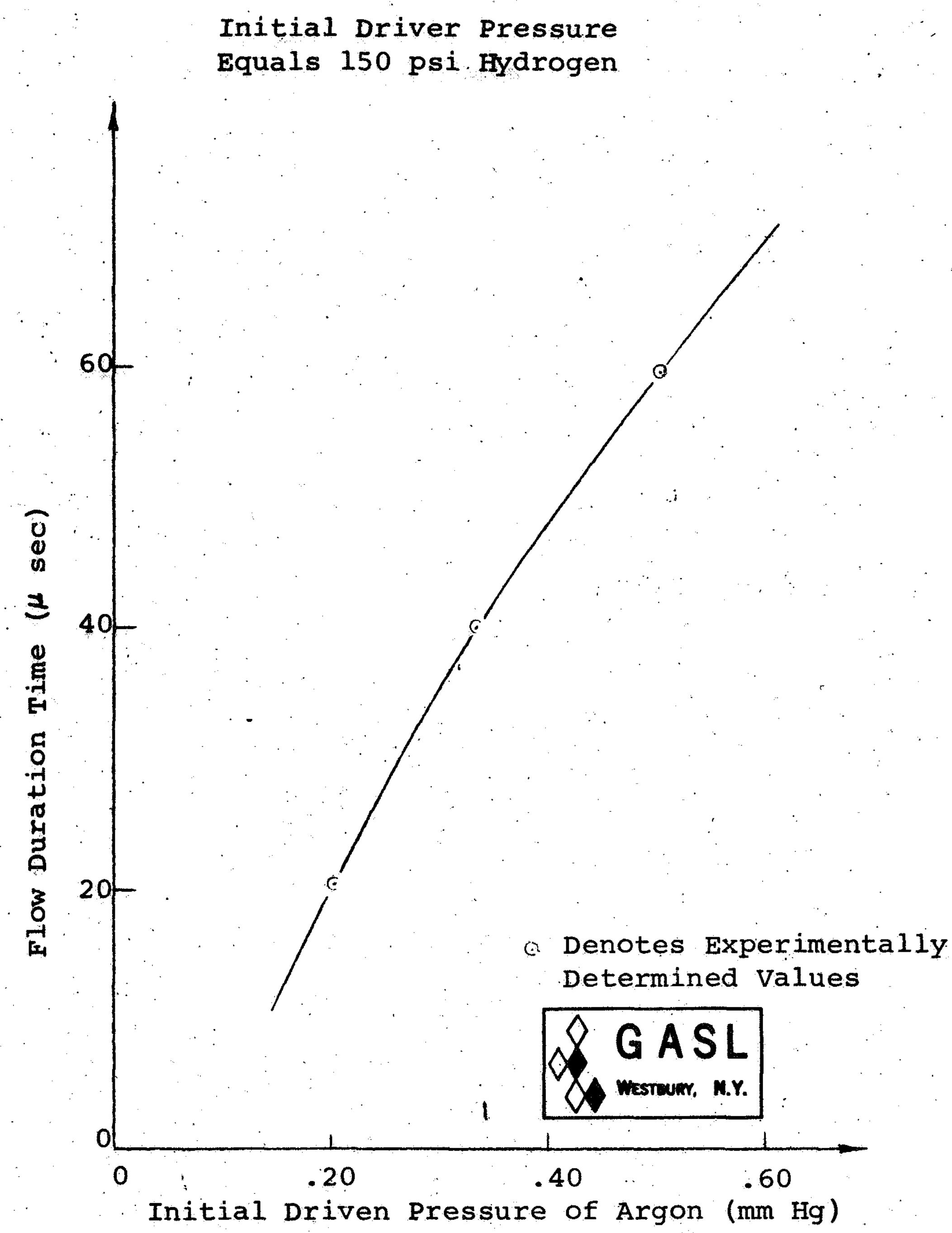

FIGURE 19. DURATION OF SHOCK PRODUCED PLASMA

NASA Contract NAS5-9881

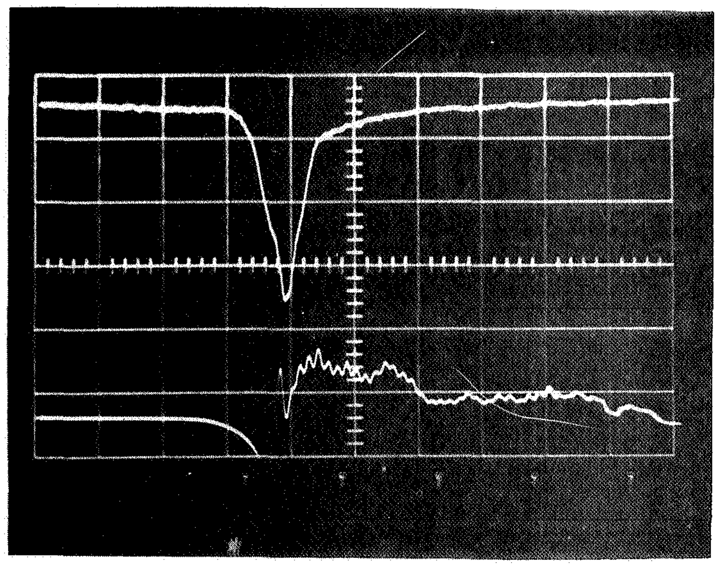

P_i=.35 mm (Hg) Argon

P_2= 150 psi Hydrogen

GASL
WESTBURY, N.Y.

FIGURE 20. FOUR mm INTERFEROMETER TRACE OF FLOW CHECKED PREVIOUSLY WITH ONE cm INTERFEROMETER

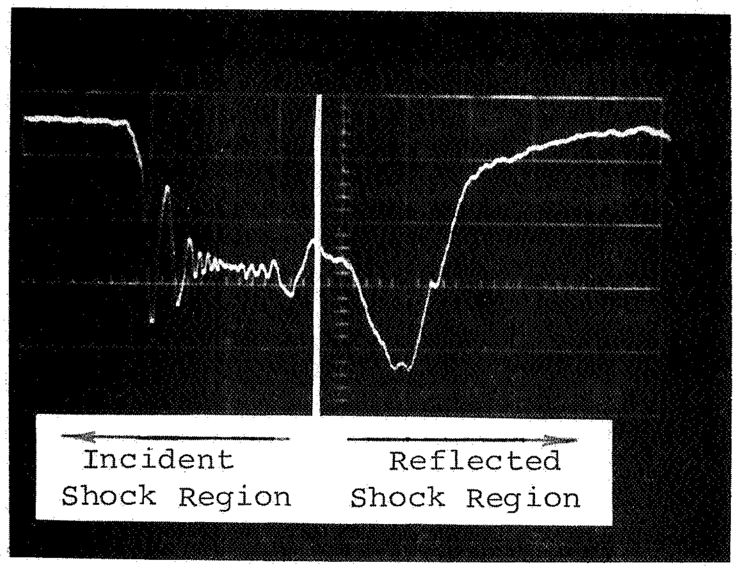

P_i=.50 mm(Hg) Argon

M=11.3

Time Scale = 10μs/cm

FIGURE 21. FOUR mm INTERFEROMETER TRACES OF INCIDENT AND REFLECTED PLASMA

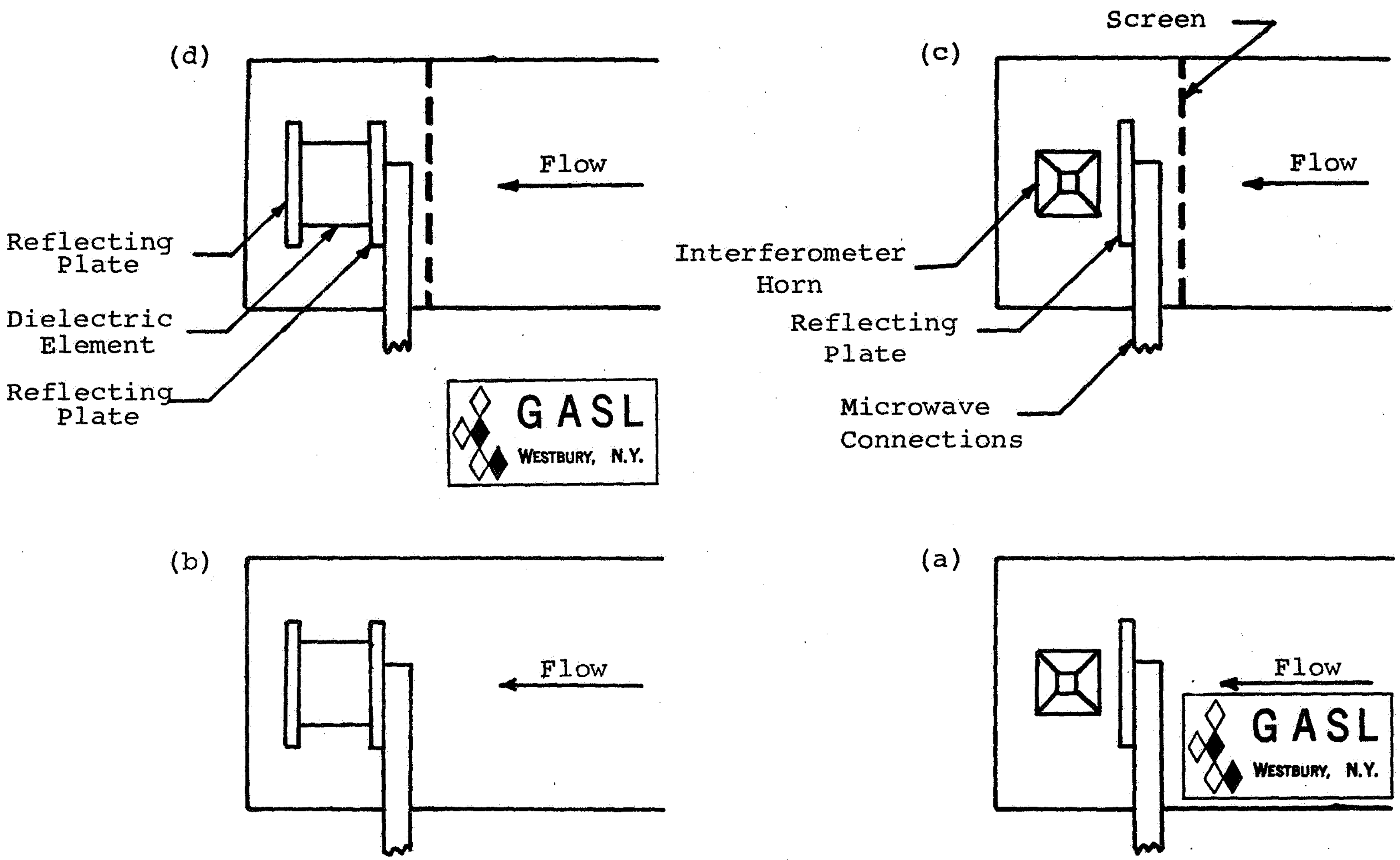

FIG. 22. HALF CYCLE (180°) PHASE SHIFT STUDIES OF REFLECTED SHOCK PLASMAS

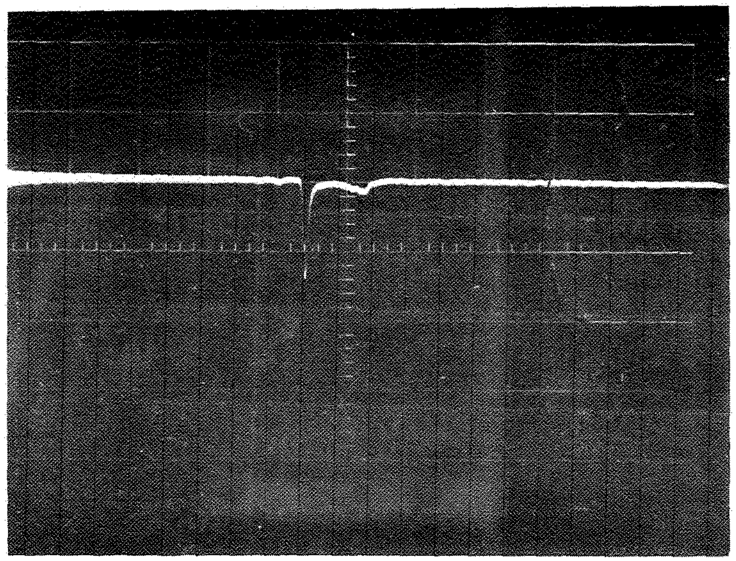

GASL
WESTBURY, N.Y.

FIG. 23. PROBE REACTION AT 700 MHz

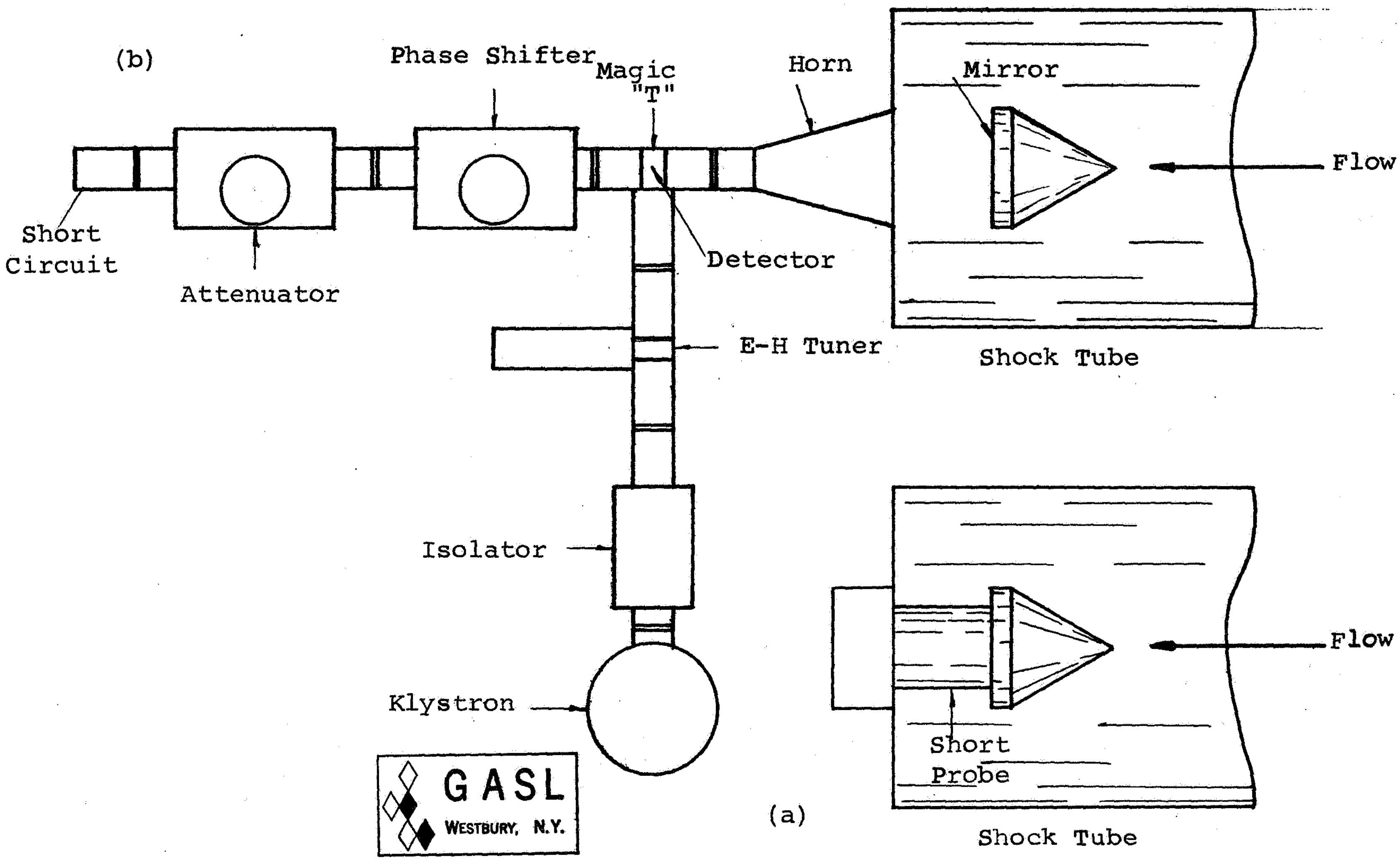

FIGURE 24. SCHEMATIC DIAGRAM OF DOUBLE-PATH INTERFEROMETER

NASA Contract NAS5-9881

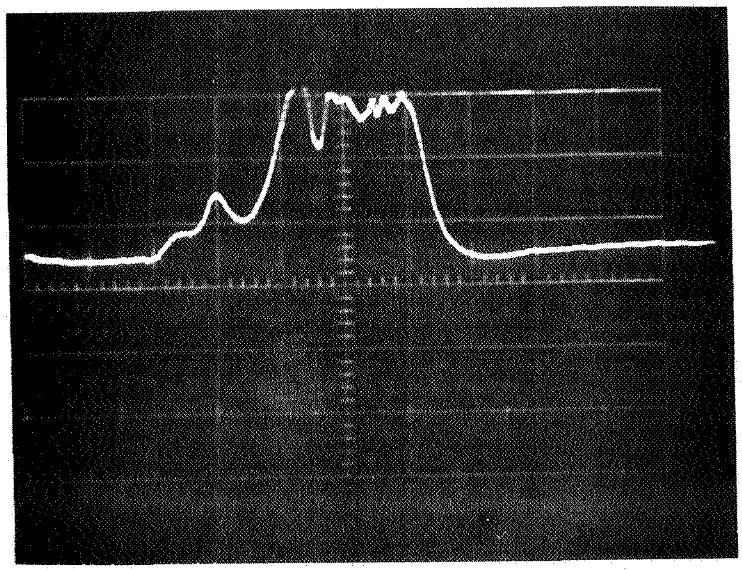

P_i = .5 mm (Hg) Argon
M = 6.0

GASL
WESTBURY, N.Y.

FIGURE 25. RESPONSE OF FOUR mm DOUBLE PATH INTERFEROMETER

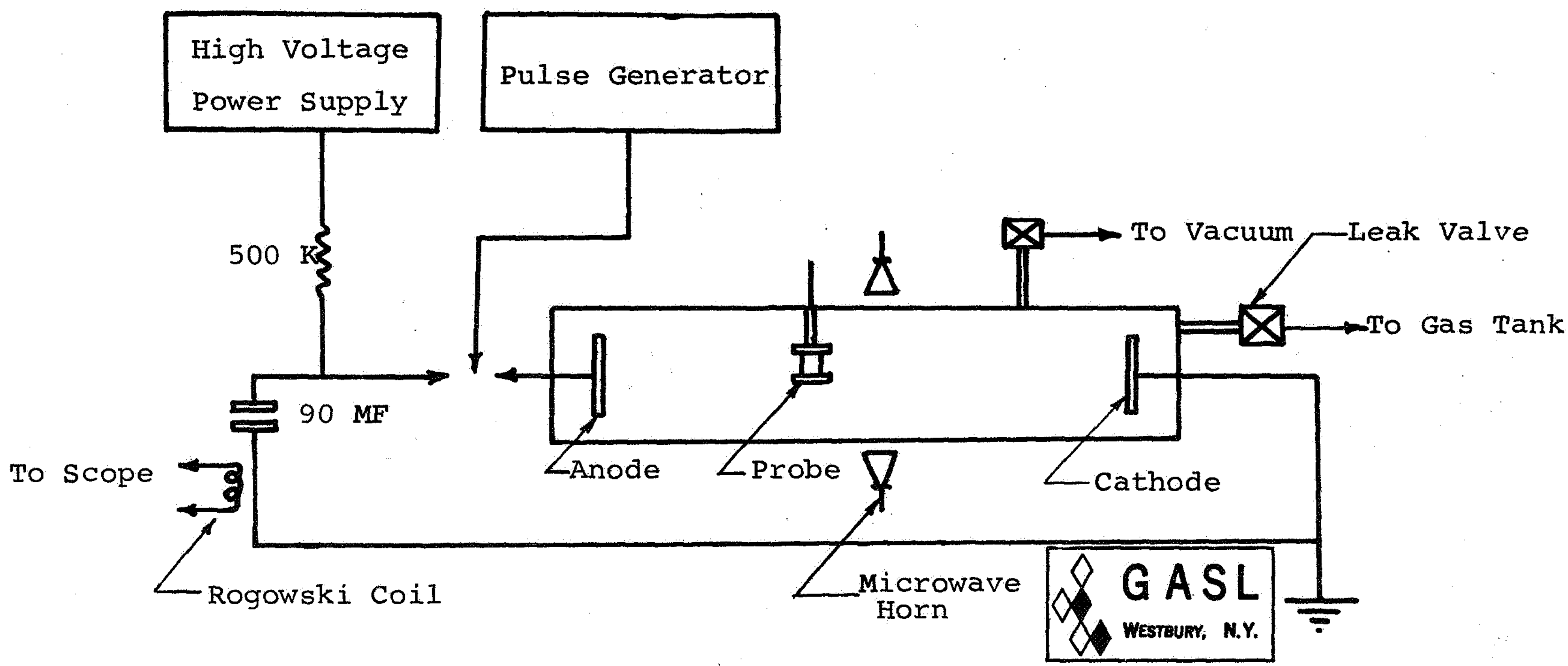

FIG. 26. DISCHARGE TUBE EXPERIMENTAL ARRANGEMENT

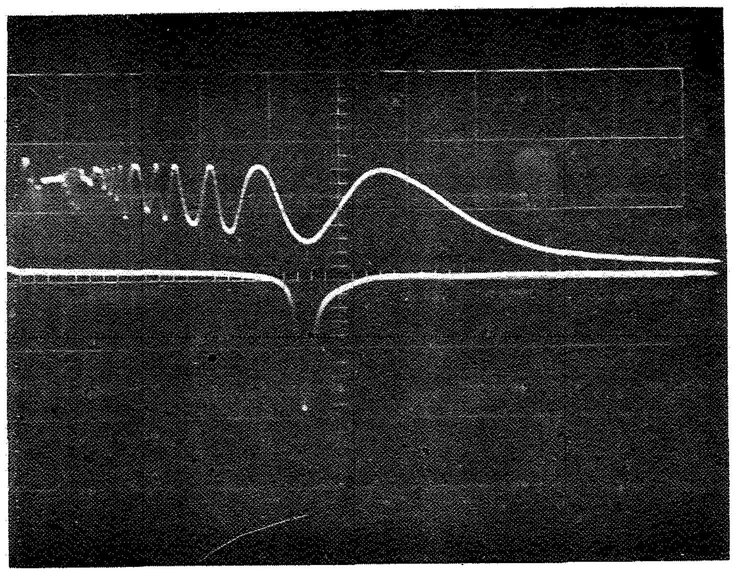

GASL
WESTBURY, N.Y.

FIG. 27. TYPICAL PROBE RESPONSE IN A DISCHARGE PRODUCED PLASMA

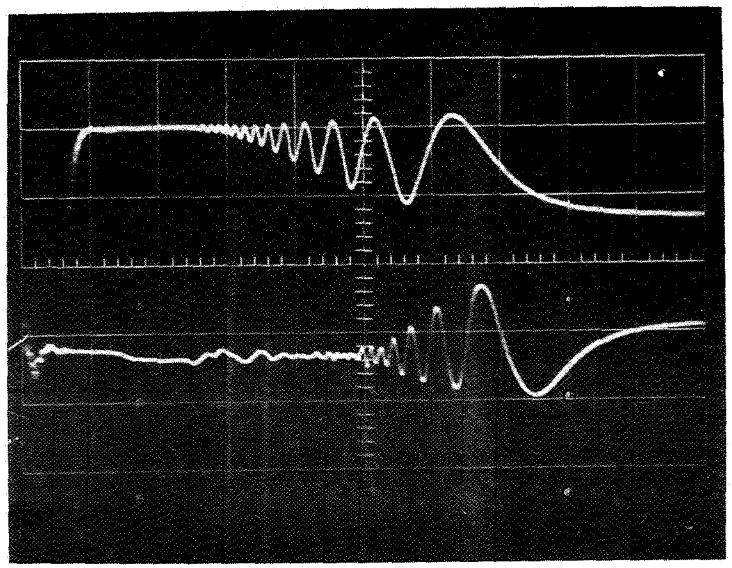

GASL WESTBURY, N.Y.

FIG. 28. COMPARISON OF INTERFEROMETERS IN A DISCHARGE PRODUCED PLASMA

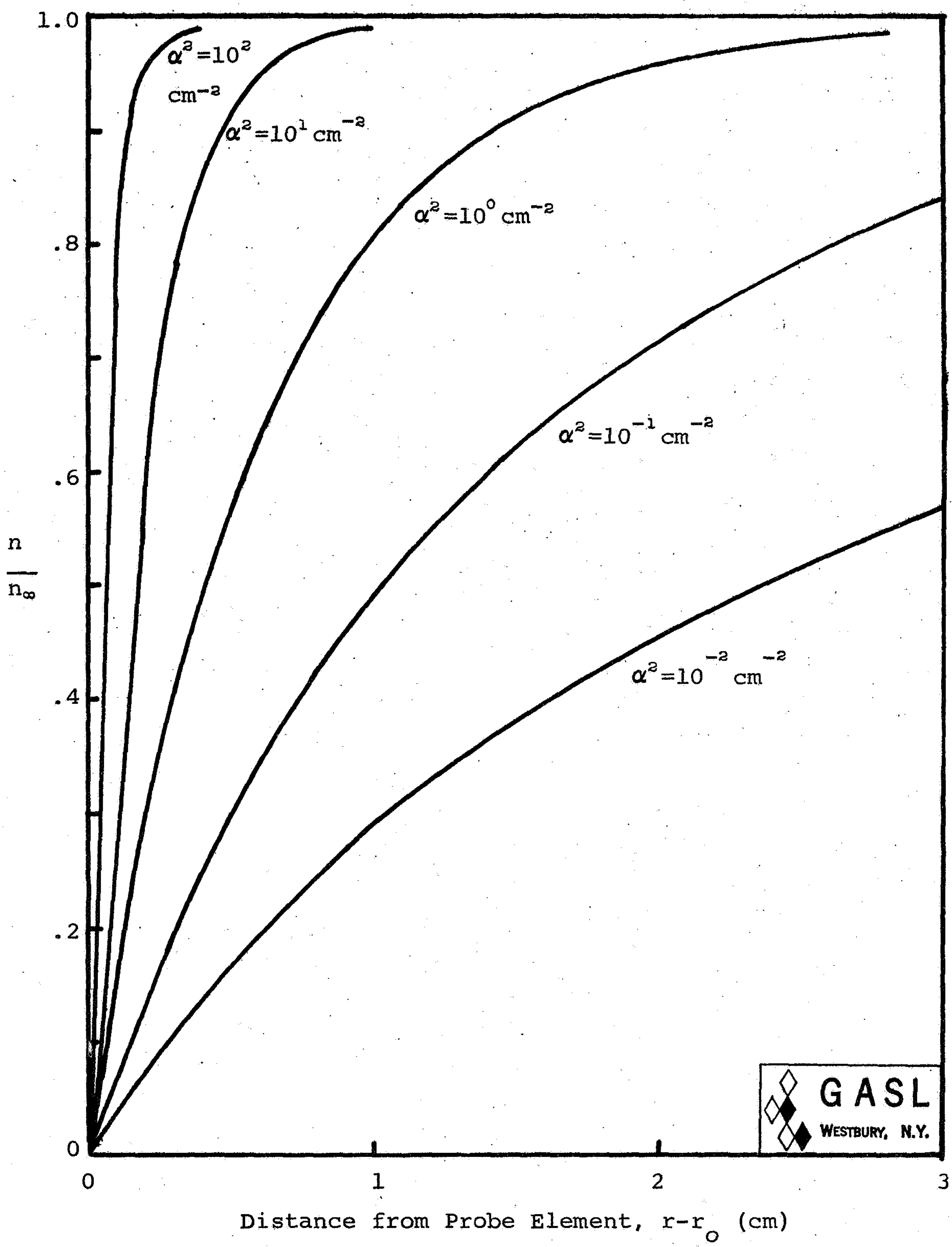

FIG. 29. EFFECT OF DIFFUSION ON THE ELECTRON DENSITY DISTRIBUTION

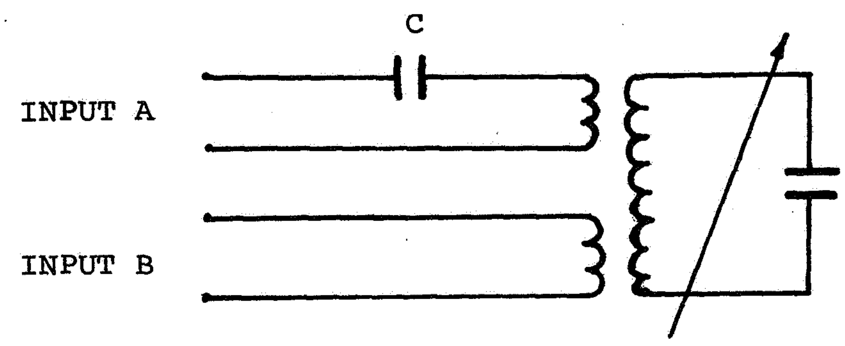

(a) Equivalent Circuit for the Probe

GASL WESTBURY, N.Y.

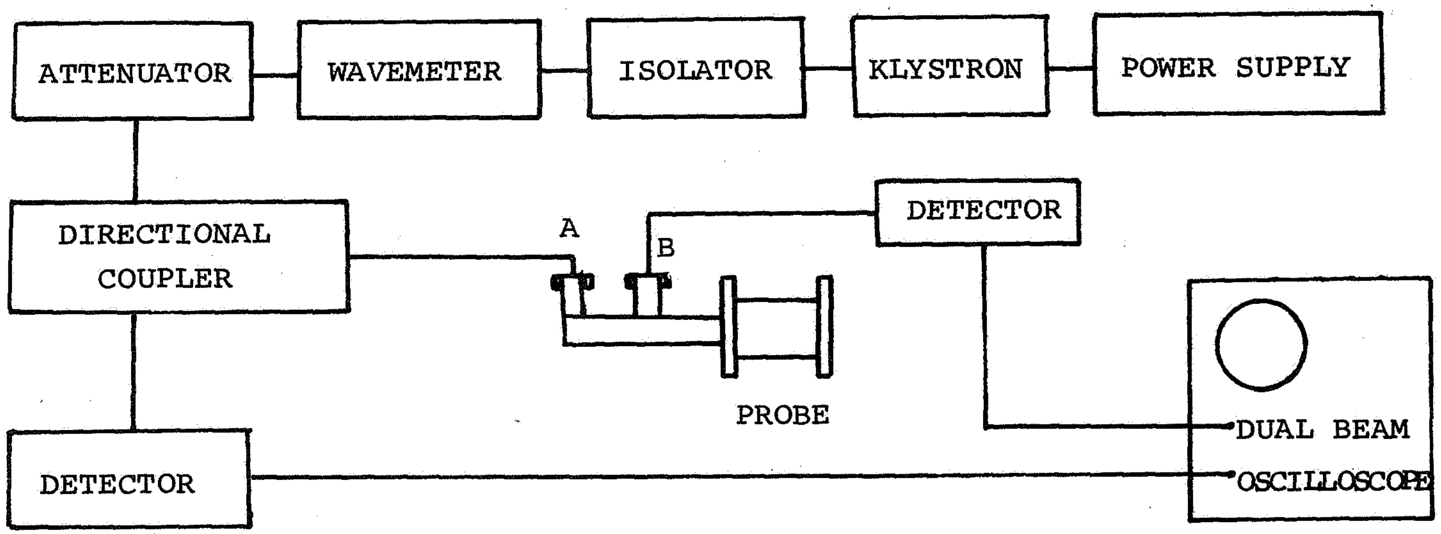

(b)

FIG. 30. TEST CIRCUIT FOR THE PROBE

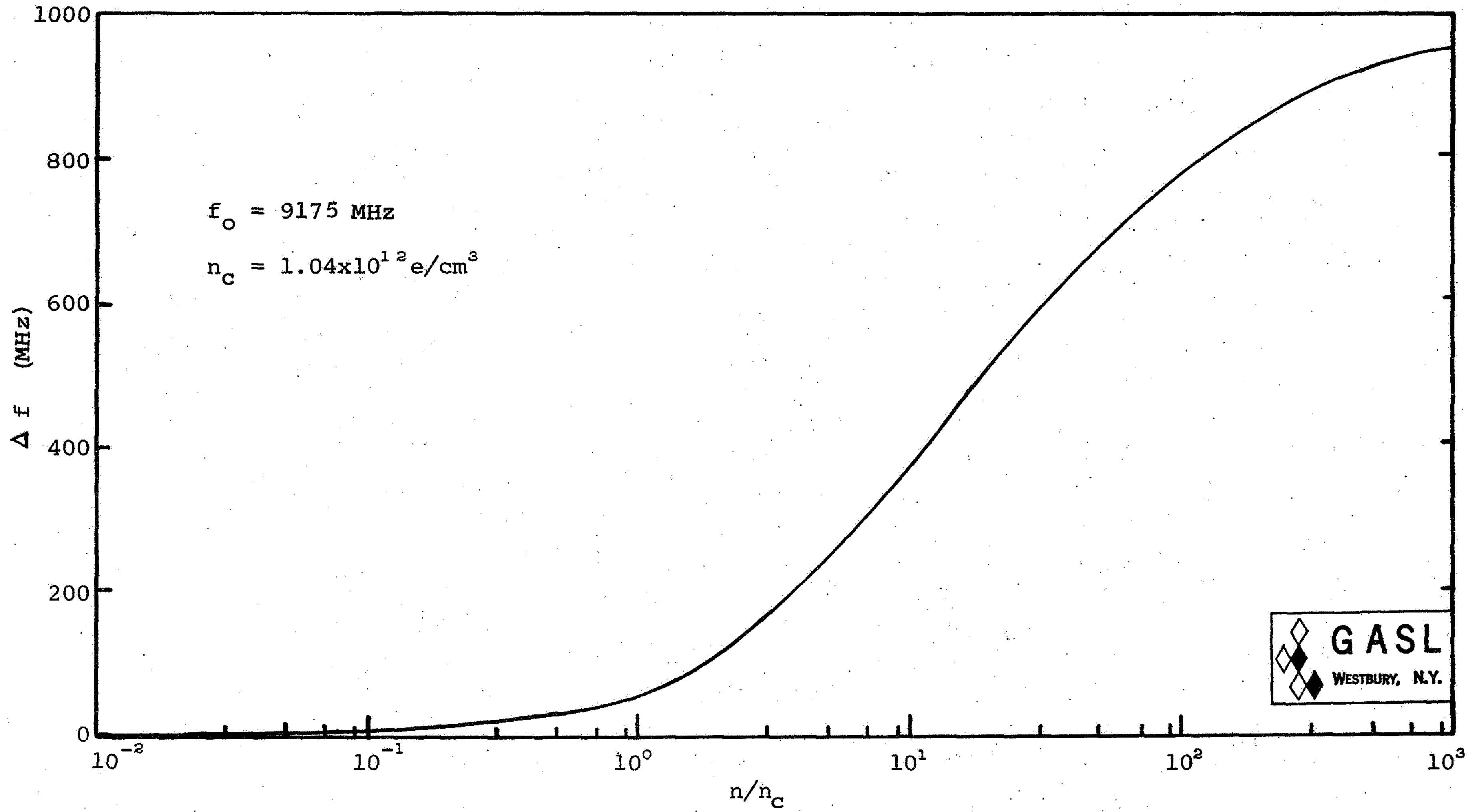

FIG. 31. FINAL CALIBRATION CURVE FOR ELECTRON DENSITY PROBE

NAS5-9881

GASL
WESTBURY, N.Y.

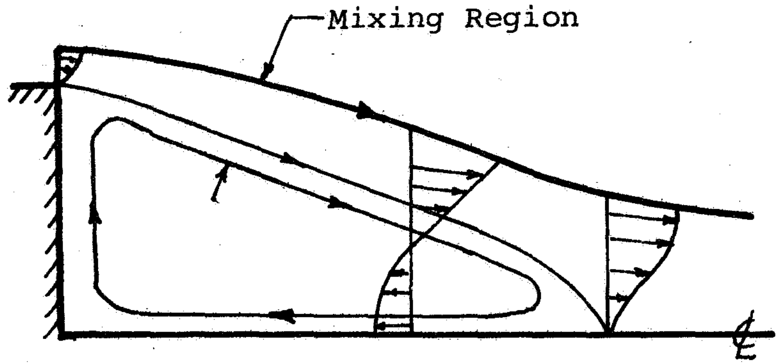

(a) High Reynolds Number Base Flow

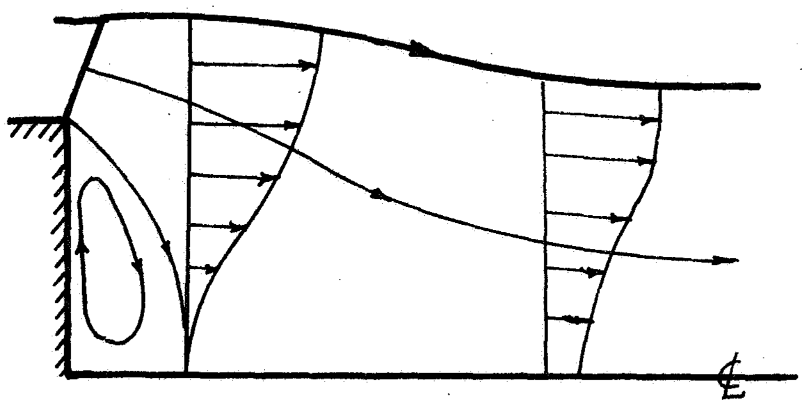

(b) Low Reynolds Number Base Flow

FIG. 32. COMPARISON OF HIGH AND LOW REYNOLDS NUMBER BASE FLOWS

GASL
WESTBURY, N.Y.

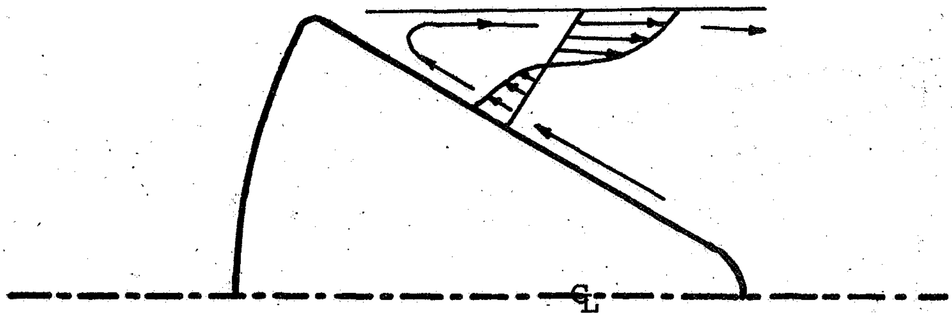

(a) High Reynolds Number

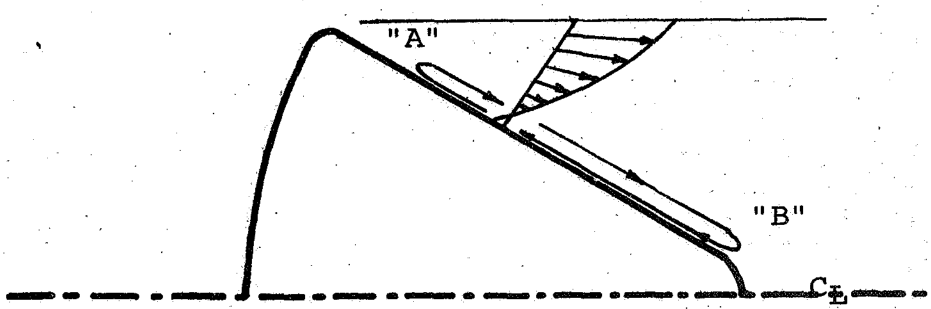

(b) Low Reynolds Number

FIG. 33. COMPARISON OF HIGH AND LOW REYNOLDS NUMBER BASE FLOW PATTERNS ASSUMED TO EXIST ON THE LEEWARD SIDE OF THE APOLLO AFTERBODY

GASL
WESTBURY, N.Y.

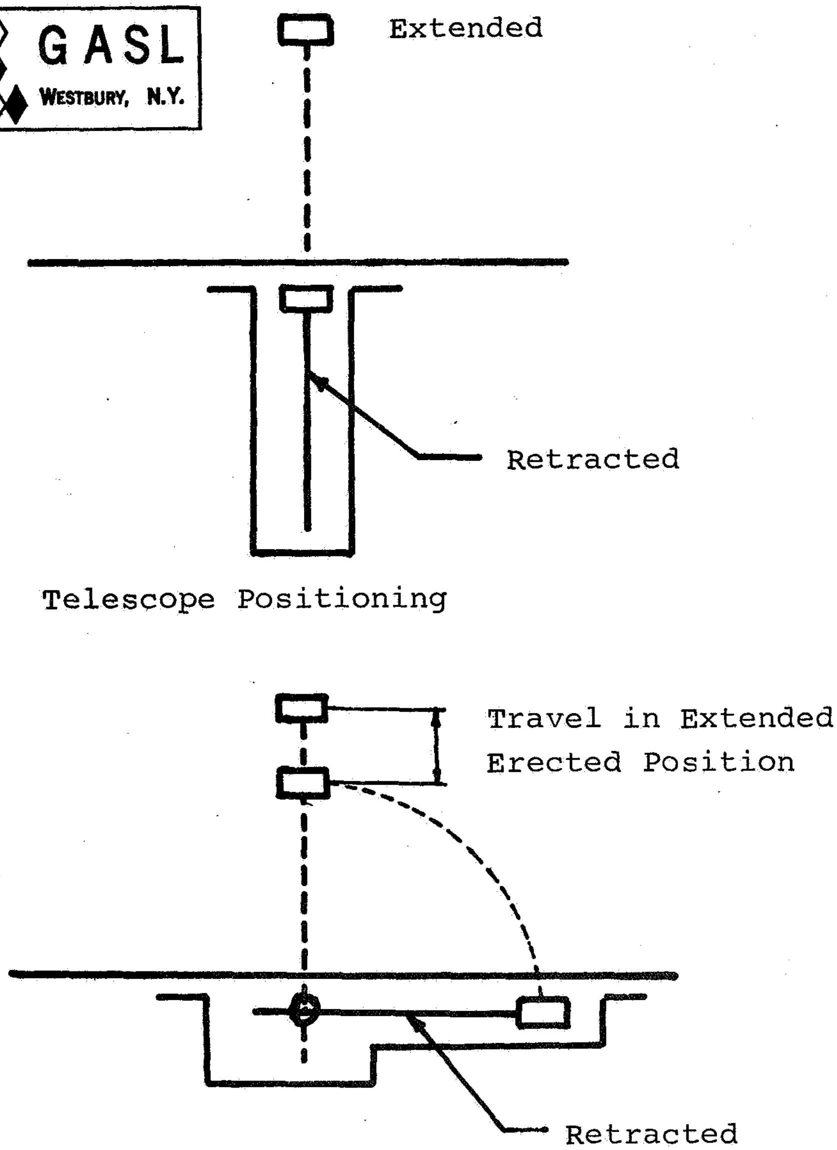

(a) Telescope Positioning

(b) Rotation for Major Portion of Required Travel

FIG. 34. SCHEMATIC DIAGRAMS OF METHODS OF PROBE EXTENSION

GASL
WESTBURY, N.Y.

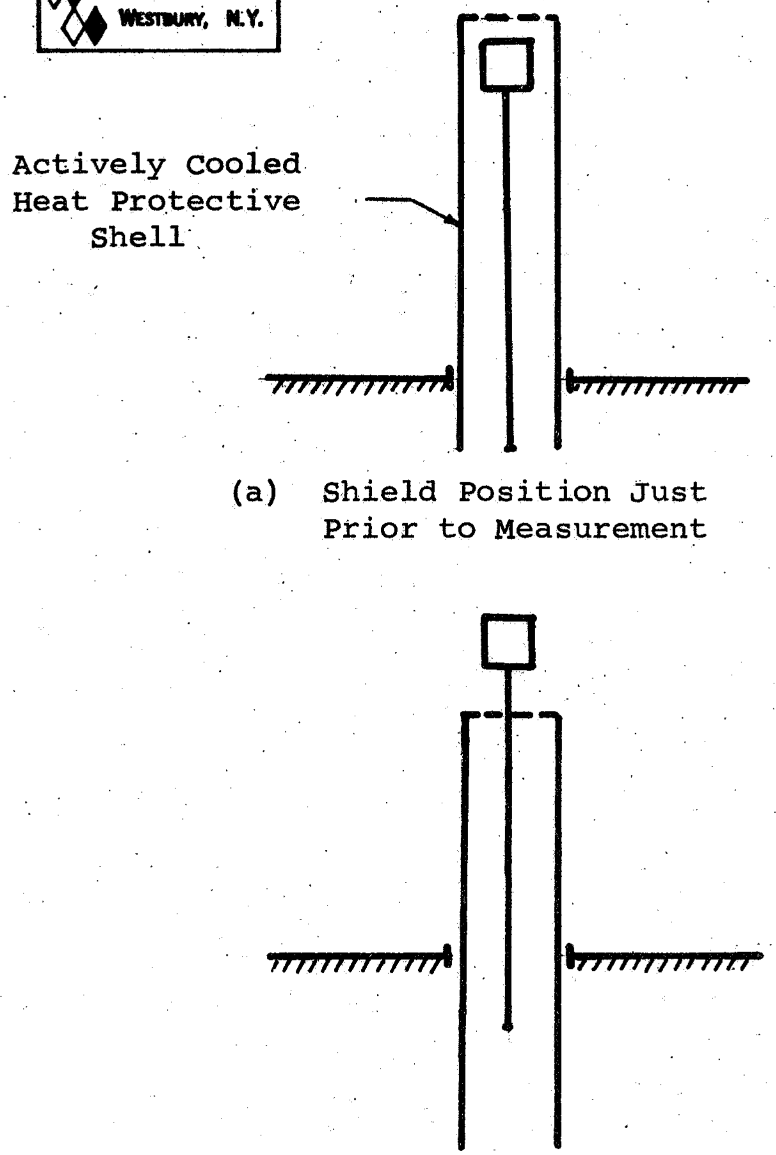

(a) Shield Position Just Prior to Measurement

(b) Shield Position During Measurement

FIG. 35. SCHEMATIC OF PROBE HEAT PROTECTION METHOD

GASL
WESTBURY, N.Y.

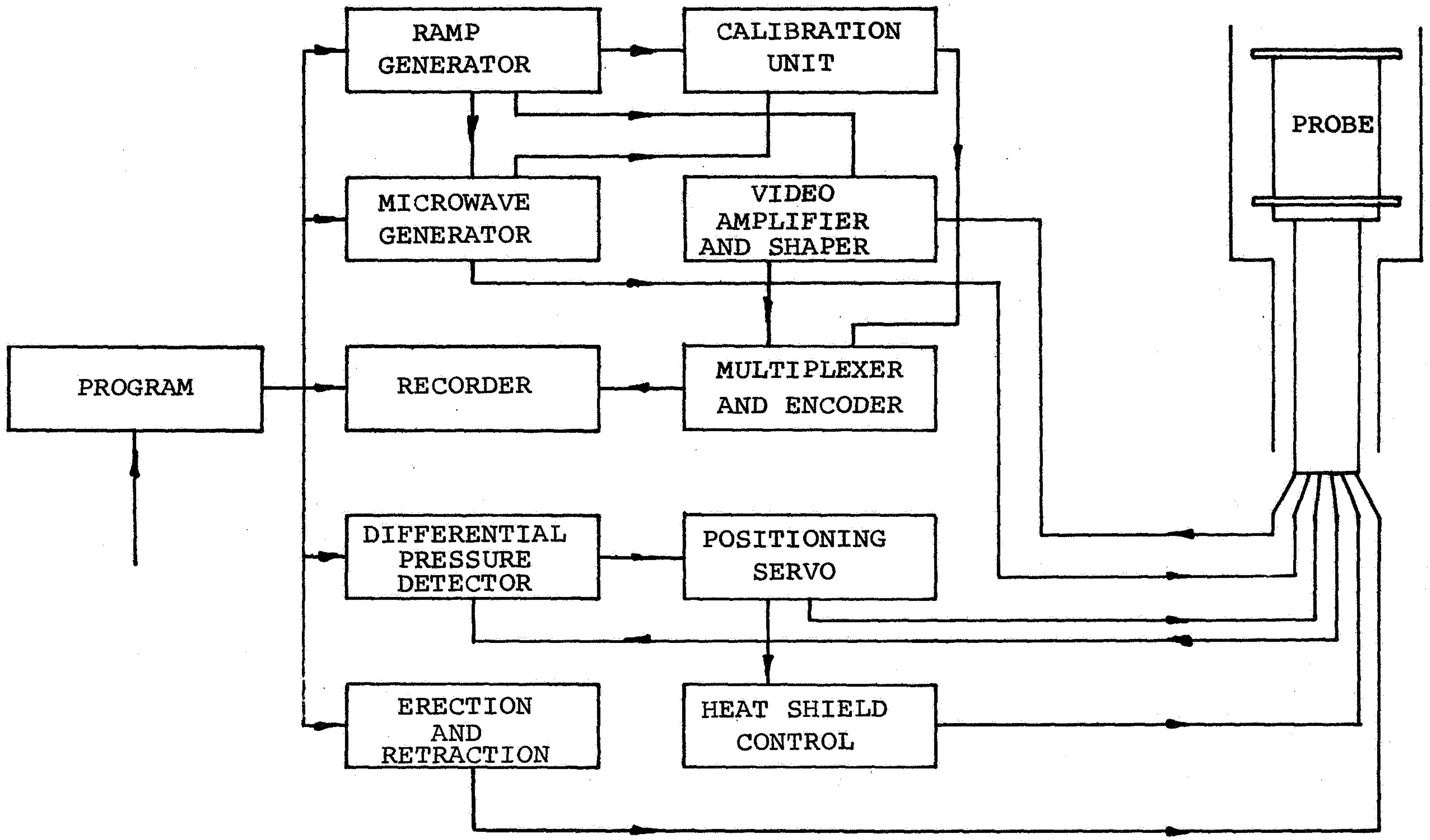

FIG. 36. MEASURING SCHEME FOR AN INFLIGHT APPLICATION

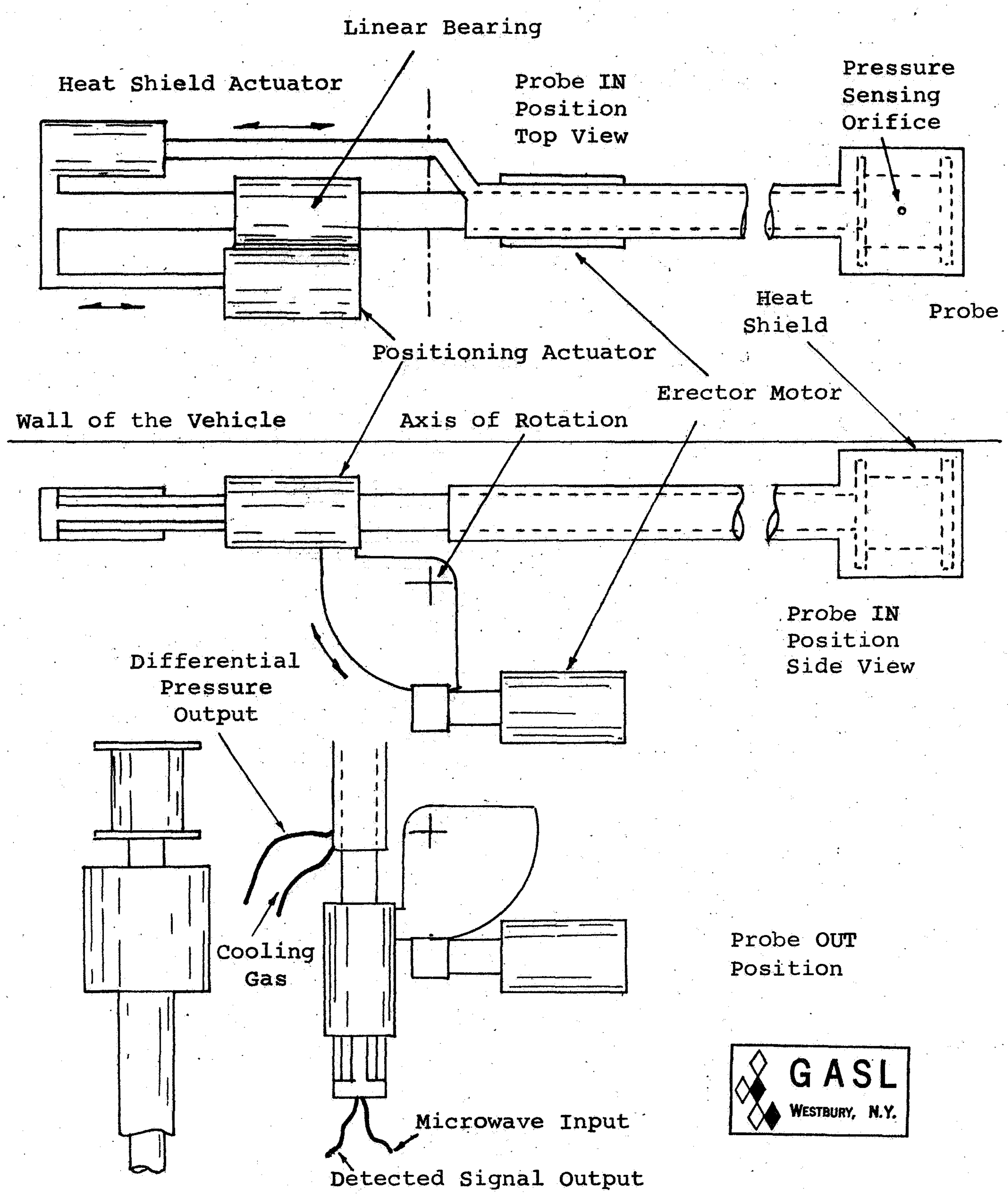

FIG. 37. PROBE POSITIONING SYSTEM

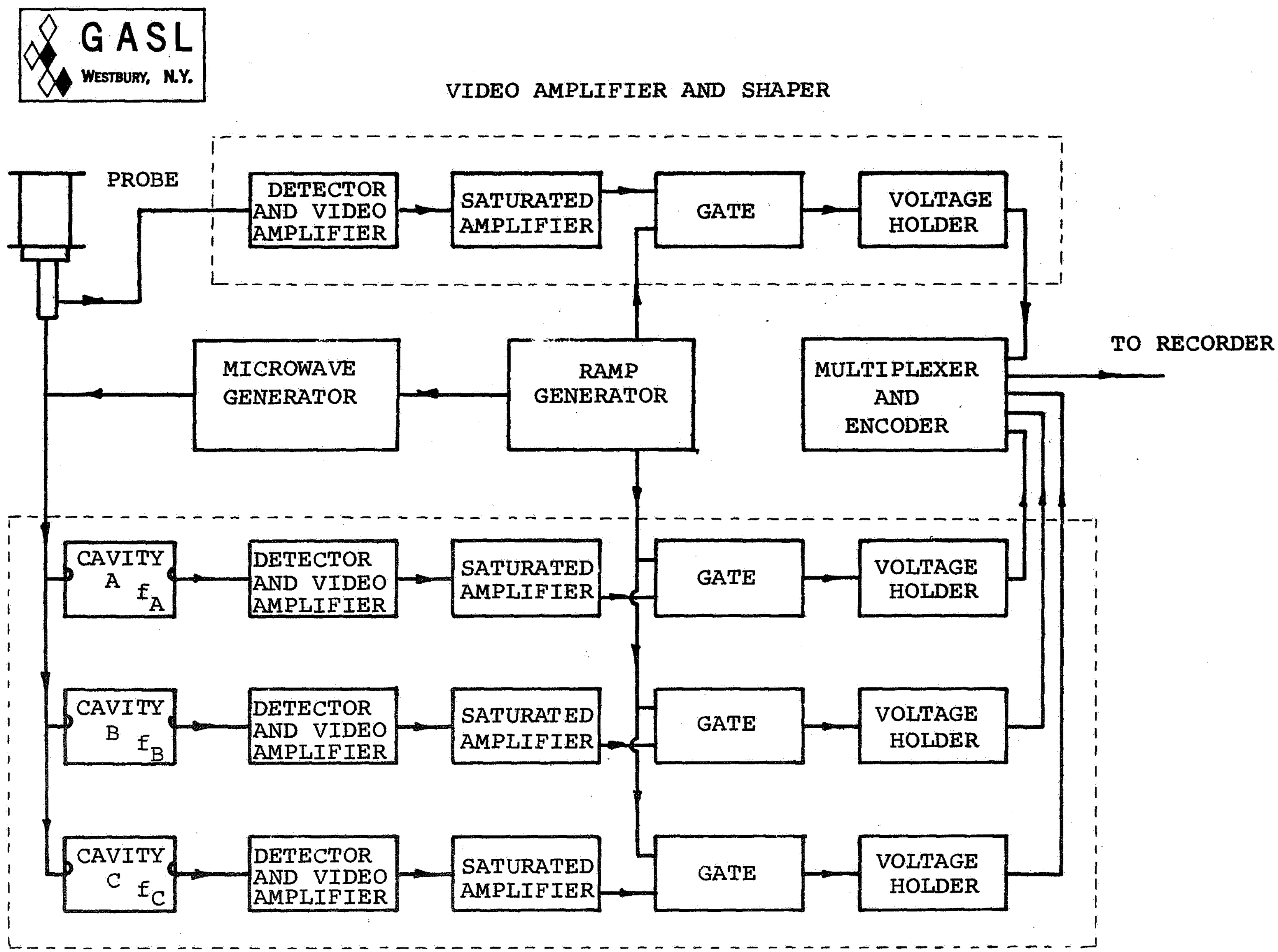

FIG. 38. ELECTRONIC CIRCUITRY FOR INFLIGHT APPLICATION

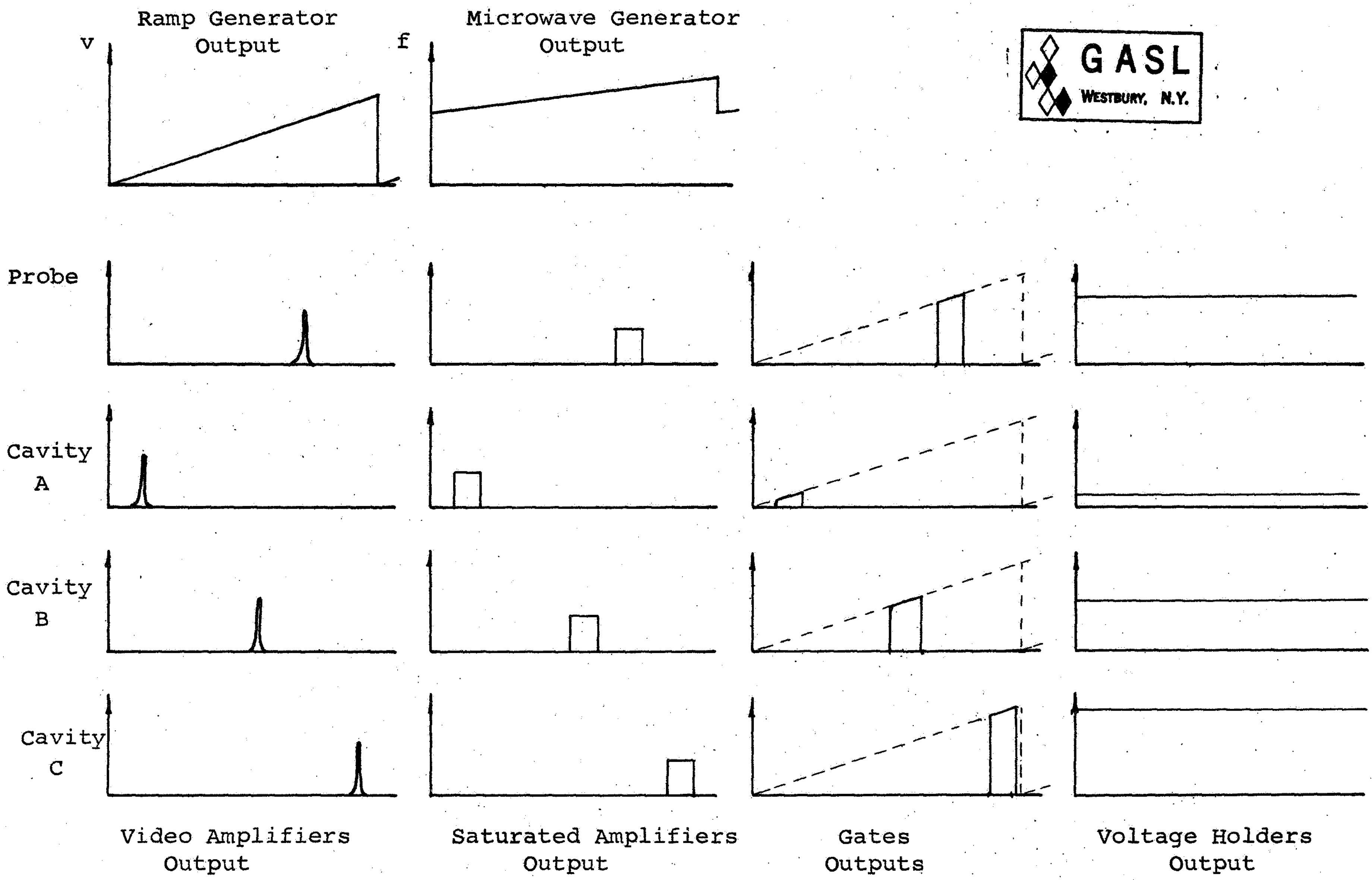

FIG. 39. WAVEFORMS IN THE ELECTRONIC CIRCUIT

APPENDIX I

Calibration with Metallic Cylinders

The equivalent electron density of a metallic cylinder placed coaxial to the probe can be found by comparing the analytically determined frequency shift for such a configuration with that found for a highly overdense plasma (see Chapter IV). For a configuration such as that shown in Fig. 11, the field components can be written as

$$\begin{cases} E_{\Phi 1} = E_1 J_1(k_1 r) \sin k_z z \\ H_{z1} = -\dfrac{k_1}{i\omega\mu_o} E_1 J_0(k_1 r) \sin k_z z \end{cases} \qquad (0 < r < r_o)$$

and

$$\begin{cases} E_{\Phi 2} = [E_2 J_1(k_2 r) + E_3 N_1(k_2 r)] \sin k_z z \\ H_{z2} = -\dfrac{k_2}{i\omega\mu_o} [E_2 J_o(k_2 r) + E_3 N_o(k_2 r)] \sin k_z z \end{cases} \qquad (r_o < r < r_1)$$

where the longitudinal propagation constant is $k_z = \dfrac{n\pi}{z_o}$, and where the radial propagation constants in the dielectric and surrounding vacuum are given by

$$k_1^2 = \frac{\omega^2 \kappa_d^2}{c^2} - \frac{n^2\pi^2}{z_o^2} \quad \text{and} \quad k_2^2 = \frac{\omega^2}{c^2} - \frac{n^2\pi^2}{z_o^2}$$

respectively.

The boundary condition to be satisfied at the wall of the metal tube ($r=r_1$) is

$$E_{\Phi 2}\Big|_{r=r_1} = 0$$

or

$$E_3 = - E_2 \left[\frac{J_1(k_2 r_1)}{N_1(k_2 r_1)} \right]$$

One then has

$$E_{\Phi 2} = E_2 \, F(k_2 r) \sin k_z z$$

and

$$H_{z2} = - \frac{k_2 E_2}{i\omega\mu_o} G\,(k_2 r)$$

where

$$F(k_2 r) = J_1(k_2 r) - \left[\frac{J_1(k_2 r_1)}{N_1(k_2 r_1)} \right] N_1(k_2 r)$$

and

$$G(k_2 r) = J_o(k_2 r) - \left[\frac{J_1(k_2 r_1)}{N_1(k_2 r_1)} \right] N_o(k_2 r)$$

Matching the fields at the interface ($r=r_o$) gives the dispersion relation

$$\frac{1}{k_1} \; \frac{J_1(k_1 r_o)}{J_o(k_1 r_o)} = \frac{1}{k_2} \; \frac{F(k_2 r_o)}{G(k_2 r_o)} \qquad \text{(A-1)}$$

where

$$\frac{F(k_2 r_o)}{G(k_2 r_1)} = \frac{J_1(k_2 r_o)\, N_1(k_2 r_1) - J_1(k_2 r_1)\, N_1(k_2 r_o)}{J_o(k_2 r_o)\, N_1(k_2 r_1) - J_1(k_2 r_1)\, N_o(k_2 r_o)} \qquad \text{(A-2)}$$

Assuming $r_1 - r_o << r_o$, which is consistent with a highly overdense plasma, and $k_2(r_1 - r_o) << 1$, one can write for the denominator in Eq. (A-2)

$$J_o(k_2 r_o)\ N_1(k_2 r_1) - J_1(k_2 r_1)\ N_o(k_2 r_o) \cong -\frac{2}{\pi k_2 r_o}$$

Taking the approximations

$$J_1(k_2 r_1) \cong J_1(k_2 r_o) + J_1'(k_2 r_o)\ k_2\ \Delta r$$

and

$$N_1(k_2 r_1) \cong N_1(k_2 r_o) + N_1'(k_2 r_o)\ k_2\ \Delta r$$

where $\Delta r = r_1 - r_o$ one can write for the numerator in Eq. (A-2)

$$J_1(k_2 r_o)\ N_1(k_2 r_1) - J_1(k_2 r_1)\ N_1(k_2 r_o) \cong [J_1(k_2 r_o)\ N_1'(k_2 r_o) - J_1'(k_2 r_o)\ N_1(k_2 r_o)]\ k_2\ \Delta r$$

i.e.

$$J_1(k_2 r_o)\ N_1(k_2 r_1) - J_1(k_2 r_1)\ N_1(k_2 r_o) \simeq \frac{2}{\pi k_2 r_o}\ k_2 \Delta r$$

Thus the dispersion relation for the system of Fig. 11 becomes

$$\frac{1}{k_1} \frac{J_1(k_1 r_o)}{J_o(k_1 r_o)} \cong - \frac{1}{k_2} (k_2 \Delta r) = - \Delta r$$

or

$$\frac{J_1(k_1 r_o)}{J_o(k_1 r_o)} \cong - k_1 \Delta r \qquad \text{(A-3)}$$

In the limiting case $\Delta r = 0$, Eq. (A-3) gives

$$J_1(k_1 r_o) = 0 \qquad \text{(A-4)}$$

or

$$k_1 r_o = x_1$$

where x_1 is the first root of Eq. (A-4). For $\Delta r \neq 0$ and $k_1 \Delta r \ll x_1$ one has

$$J_1(k_1 r_o) \cong J_1(x_1) - J_1'(x_1)\, \delta$$

where

$$k_1 r_o = x_1 - \delta$$

Near the root of Eq. (A-4) one can take

$$J_1'(k_1 r_o) \cong J_o(k_1 r_o)$$

so that

$$J_1(k_1 r_o) \cong - J_o(k_1 r_o)\, \delta$$

or

$$\frac{J_1(k_1 r_o)}{J_o(k_1 r_o)} \cong - \delta \qquad \text{(A-5)}$$

Comparing this result with Eq. (A-3) one has

$$\delta \cong k_1 \ \Delta r$$

then

$$k_1 \ \Delta r = x_1 - k_1 \ r_o$$

In the limiting case $\Delta r = 0$, the resonant frequency is given by

$$\omega_1 = \frac{c}{\varkappa_d} \sqrt{\frac{n^2 \pi^2}{z_o^2} - \frac{x_1^2}{r_o^2}}$$

Expanding $k_1 \Delta r$ about this value for small Δr one has

$$k_1 \Delta r \cong x_1 - r_o \left(\frac{\omega_1^2 \ \varkappa_d^2}{c^2} - \frac{n^2 \pi^2}{z_o^2} + \frac{2\omega_o \Delta \omega \ \varkappa_d^2}{c^2} \right)^{\frac{1}{2}}$$

$$k_1 \Delta r \cong x - x_1 \left[1 + \frac{2\omega_1 \varkappa_d^2}{2c^2} \frac{\Delta \omega}{\left(\frac{\omega_1^2 \ \varkappa_d^2}{c^2} - \frac{n^2 \pi^2}{z_o^2} \right)} \right]$$

$$k_1 \Delta r \cong - \frac{\omega_1 r_o^2 \ \varkappa_d^2 \ \Delta \omega}{x_1 \ c^2}$$

Then

$$\frac{\Delta\omega}{\omega_1} = - \frac{x_1^2 c^2 \Delta r}{\omega_1^2 r_o^3 \varkappa_d^2} \qquad \text{(A-7)}$$

When the probe is located in a highly overdense lossless ($\nu = 0$) plasma the dispersion relation (see Chapter 4) is

$$\frac{\Delta\omega}{\omega_1} \cong - K_{s_1} \frac{\omega_1}{\omega_p} = - \frac{x_1^2 c^3}{\omega_1^2 r_o^3 \varkappa_d^2 \omega_p} \qquad \text{(A-8)}$$

By comparing Eq. (A-7) with (A-8) one sees that an equivalence is obtained between the dielectric rod surrounded by the metallic cylinder and the dielectric rod surrounded by a highly overdense plasma when

$$\Delta r = \frac{c}{\omega_p} \qquad \text{(A-9)}$$

It is clear that the equivalence expressed by Eq. (A-9) is valid in the asymptotic situation of extremely high electron densities.

In the range of electron densities between 10^{13} and 10^{14} e/cm^3 the penetration depth c/ω_p corresponds to the range

$$.5 < \Delta r < 1.7 \text{ mm}$$

thus Δr is a small fraction of the probe diameter and furthermore smaller than the difference between the radius of the reflector and the radius of the dielectric rod. For these reasons the equivalence between the penetration depth in the plasma and the radial distance of the metallic wrapping can be used for the probe calibration in the upper electron density range.

PROJECT 8029

Distribution List for Final Report
NASA Contract NAS5-9881

National Aeronautics & Space Administration
Goddard Space Flight Center
Glenn Dale Road
Greenbelt, Maryland 20771

		No. Cys.
Attn:	Office of the Director, Code 100	1
Attn:	Office of the Ass't Director SS&SA, Code 600	3
Attn:	Office of the Ass't Director T&DS, Code 500	3
Attn:	Office of Technical Services, Code 300	3
Attn:	Library, Code 252	2
Attn:	Mr. M. C. Saunders, Code 248	2
Attn:	Technical Information Division, Code 250	4
Attn:	Dr. Richard Lehnert, Code 513	102 and 1 reproducible